PROCEEDINGS A

royalsocietypublishing.org/journal/rspa

Research

Cite this article: Torres-Ulloa C, Grassia P. 2023 Viscous froth model applied to multiple topological transformations of bubbles flowing in a channel: three-bubble case. *Proc. R. Soc. A* **479**: 20220785. https://doi.org/10.1098/rspa.2022.0785

Received: 23 November 2022
Accepted: 7 June 2023

Subject Areas:
applied mathematics, fluid mechanics, topology

Keywords:
viscous froth model, physics of bubbles, foam rheology, topological transformations

Author for correspondence:
Paul Grassia
e-mail: paul.grassia@strath.ac.uk

Viscous froth model applied to multiple topological transformations of bubbles flowing in a channel: three-bubble case

Carlos Torres-Ulloa[1,2,3] and Paul Grassia[1]

[1]Department of Chemical and Process Engineering, University of Strathclyde, James Weir Building, 75 Montrose Street, Glasgow G11XJ, UK
[2]Centro de Investigación, Innovación y Creación (CIIC), Universidad Católica de Temuco, Rudecindo Ortega' 03690, Temuco, Chile
[3]Departamento de Ciencias Matemáticas y Físicas, Facultad de Ingeniería, Universidad Católica de Temuco, Rudecindo Ortega 03694, Temuco, Chile

PG, 0000-0001-5236-1850

A two-dimensional foam system comprised of three bubbles is studied via dynamic simulations with the viscous froth model. The bubbles are arranged in a staircase configuration and move along a channel due to an imposed driving back pressure. Depending on the bubble size relative to channel size, the three-bubble system can undergo topological transformations (as for a simpler staircase structure, known as the simple lens) or it can reach a geometrically invariant migrating state (as for an infinite staircase structure). A methodology used previously determined the system evolution up to the first topological transformation, but evolution beyond this was not studied before. To address this, unsteady state three-bubble simulations are realized here, extending beyond the first transformation. For sufficiently high imposed back pressures, a sequence of topological transformations occurs before a steadily migrating shape is reached, typically in a topology such that an equal number of films connect to both channel walls.

Electronic supplementary material is available online at https://doi.org/10.6084/m9.figshare.c.6708076.

THE ROYAL SOCIETY PUBLISHING

1. Introduction

Interaction with liquid foam (a dispersion of gas in a liquid surfactant solution) in our daily life is unavoidable, and in addition foam is encountered in various fields, such as the food industry, manufacturing of ultra-light materials, development of medical procedures, in the manufacture of some pharmaceutical products, detergents, cosmetics, in the oil recovery industry, in recovery and production of minerals, and also as a firefighting agent [1–4]. Applications in which the foam is made to flow in specific geometries, such as a porous medium or confined channels [5,6], are of particular interest for this work. In such applications, a key parameter to determine the dynamics of the foam flow is the mobility, which determines for a specified driving back pressure, how fast a foam with a specific bubble configuration moves within a channel of specific geometry [7]. Foam mobility depends, in turn, on variables like the bubble size distribution and configuration within the channel of transport, roughness of the channel walls, viscosity of the liquid and gas phases and surface tension between them, liquid fraction of the foam and the number of individual bubbles flowing together [7]. However, an important point just mentioned here is that mobility is sensitive to bubble configuration [8,9], so that if the configuration ever changes for a given set of bubbles, the mobility must change too. Hence knowing about any changes in bubble configuration is important [10]. It has been observed that changing the driving pressure can cause bubble configuration to change [11–13]. That, in turn, influences mobility and hence changes the velocity of propagation for the set specified pressure. These sorts of pressure-induced configurational changes and how they influence foam flow in confined channels are then the topics to be explored here.

Changes in bubble configurations specifically involve bubble neighbour exchanges, also known as $T1$ topological transformations [14]. Previous work [15,16] has, therefore, focused on how a foam structure that propagates along a channel might either undergo $T1$ or resist $T1$, albeit this was done in the specific case of a 'foam' consisting of just three bubbles. The reason for selecting a three-bubble system in particular is that it admits a variety of topological transformation behaviour, and (in a sense to be made precise later) sometimes behaves akin to a system with very few bubbles and sometimes behaves akin to a system with many bubbles. Three bubbles, therefore, constitute a rich physical system that can offer insights also into systems containing various different numbers of bubbles: this then is the basis for choosing to study three bubbles.

How bubble sizes relative to channel size impact on the tendency of three-bubble systems to undergo or not undergo topological transformations, i.e. how bubble sizes affect the system's susceptibility or resilience to $T1$, is then what [15,16] studied. However, those studies considered susceptibility or resilience to $T1$ starting from just one particular topological configuration. What we study in the present work, however, is how bubble sizes coupled with distinct topological configurations attained following a $T1$, might or might not lead to further $T1$s and hence a sequence of even more configurations. In other words, we explore how the topological configuration itself might affect a system's level of resilience to $T1$. Knowing about resilience to $T1$s of each distinct topology is of interest, since once a definitive topological configuration is attained that is more resilient than any of its predecessors, that configuration then governs, as mentioned above, the foam's mobility, and so ultimately governs foam flow in confined channels.

Background about the system to be studied, how topological transformations arise, and more justification behind choosing to consider the three-bubble system in particular are given in the next section. The specific open questions that will be addressed for that three-bubble system are also detailed within §2. The remainder of this study is then structured as follows. In §3, we introduce the topological transformation paths that the simulation results indicate the three-bubble system is allowed to follow after the first topological transformation. The simulation results themselves are presented in §4, and conclusions are offered in §5. Further discussions and analysis are relegated to the electronic supplementary material.

2. Foam flows in confined channels

The challenges of modelling how foam flows within a confined geometry can be simplified by considering two-dimensional foam systems contained e.g. in a Hele-Shaw cell [17,18]. In this type of container, the foam is a monolayer confined between two glass plates with a small separation in comparison both with the cell width and with the extent of the plates along the flow direction [17]: see the sketch in figure S1 in the electronic supplementary material. Therefore, when seen from above the top plate, the bubble films in the foam monolayers appear to be curves of negligible thickness (figure 1). Moreover in the two-dimensional view in figure 1, we see what appear to be upper and lower channel walls. In reality they are sidewalls across the width of the Hele-Shaw cell, but when working in a two-dimensional view as is the case throughout here, it is convenient to designate them instead as upper and lower, and that is the terminology that we adopt later on.

Two-dimensional foam systems confined in channels, particularly systems with bubbles arranged in a staircase configuration zig-zagging across the channel, are of relevance for this study (see figure 1; in particular figure 1*b* is a very long staircase, whereas figure 1*a* is a drastic truncation thereof). In the dry limit [20], which is what we consider here, the foam structure is delineated via the films between bubbles. The size of each bubble is determined by the area enclosed by its films, and is considered to be fixed over time, regardless of how the bubble moves. Note that areas are fixed since diffusive coarsening of the bubble area is not relevant on time scales of interest (see the electronic supplementary material, section S1, for an indication of the time scales involved). These bubble areas can also be compared with a characteristic scale for area, which is the square of the width of the channel. Bubble films meanwhile are driven by pressure, are subject to surface tension forces, and also experience viscous drag [8] since they move relative to the confining channel. Taken together all these various forces constitute a so-called viscous froth model [21]: see the electronic supplementary material, section S1, for details. The bubble films are known moreover to meet three by three at vertices subtending angles of 120° (or $2\pi/3$), and can also be taken to meet the channel walls subtending angles of 90° (or $\pi/2$): for details see [19].

In what follows, we describe the particular system to be studied here (§2a), open questions that we address (§2b) and the strategy for tackling those questions (§2c).

(a) Three-bubble system

The three-bubble system shown in figure 1*c* is what we consider here. Full details of how the three-bubble system is configured can be found in [15,16]. However for the convenience of the reader, these details are in the electronic supplementary material, section S2. For the moment though, we just mention that bubbles are numbered $\mathcal{B}_1$, $\mathcal{B}_2$ and $\mathcal{B}_3$, where the numbers are assigned from left to right in figure 1*c*. Bubbles $\mathcal{B}_1$ and $\mathcal{B}_3$ are by assumption the same size. Vertices V_1, V_2 and V_3, at each of which three films meet, are numbered (like the bubbles themselves) left to right. At equilibrium, distances from vertices V_1 and V_2 to the upper channel wall are denoted l_1° and l_2°, and in addition V_3 is at the same distance from the upper channel wall as V_1. Here also l_1° and l_2° are taken as dimensionless quantities, with the distance between the upper and lower channel walls being treated as the unit of distance. The quantities l_1° and l_2° (with $l_2^\circ \leq l_1^\circ$ always) are just surrogates for bubble areas [15]. Increasing l_1° increases the size of bubbles $\mathcal{B}_1$ and $\mathcal{B}_3$. Increasing l_2°/l_1° decreases the size of bubble $\mathcal{B}_2$.

A driving back pressure p_b (typically made dimensionless on a scale associated with capillary effects; see section S1 in the electronic supplementary material for details) is now imposed on the three-bubble system. This then sets it into motion and out of equilibrium: it is the viscous drag forces in the moving system which causes it to depart from equilibrium. In this context, the driven system has been studied before [15,16] via both steady and unsteady state approaches (see sections S3 and S4 in the electronic supplementary material). The steady state system, as modelled by Torres-Ulloa & Grassia [15], corresponds to driving the system with an imposed pressure that is increased from zero only very gradually: it looks for steadily propagating solutions

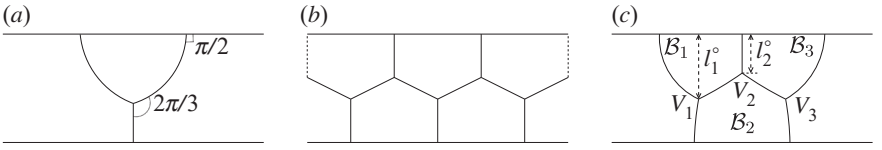

Figure 1. Foam structures in a confined straight channel, looking down at a Hele-Shaw cell from above, so the upper and lower channel walls are in fact sidewalls of the original Hele-Shaw cell. Bubble films obey Plateau's laws: they connect three by three in vertices subtending an angle of 120° (or $2\pi/3$), and meeting the cell's boundaries forming an angle of 90° (or $\pi/2$), even when the foam is set into motion [19]. (*a*) Simple lens. (*b*) Infinite staircase. (*c*) Three-bubble system, with bubbles $\mathcal{B}_1$, $\mathcal{B}_2$ and $\mathcal{B}_3$ being numbered from left to right. Here bubbles $\mathcal{B}_1$ and $\mathcal{B}_3$, both attached to the upper channel wall, are by assumption of the same size, but bubble $\mathcal{B}_2$ attached to the lower channel wall might be of different size. Assuming the distance across the channel is one dimensionless unit, l_1° and l_2° are the dimensionless distances from vertices V_1 and V_2 (also numbered left to right) to the upper channel wall in an equilibrium state. Vertex V_3 is at the same distance from the upper channel wall as vertex V_1, at least at equilibrium. The quantities l_1° and l_2° are used as surrogates of bubble areas. The simple lens is a drastically truncated version of the infinite staircase, whereas the three-bubble case interpolates between those two systems. Both the simple lens and three-bubble system are asymmetric, in the sense that unequal numbers of films attach to the upper and lower channel walls.

at each imposed pressure. Like the pressures themselves, the steady velocities that result can be made dimensionless as per the electronic supplementary material, section S1. In steadily propagating states, the apparent velocity v along the channel direction of each film element must be uniform over the entire structure. The unsteady state system meanwhile, as modelled and simulated by Torres-Ulloa & Grassia [16], corresponds to imposing a driving pressure suddenly. The system starts off at rest, but begins to evolve once the driving pressure is imposed. There is no requirement for uniform velocity while the evolution still occurs.

Via both methodologies, the three-bubble system (at least with certain bubble size distributions) is found to reach $T1$ topological transformations when a sufficiently high imposed back pressure is imposed. The physical mechanism behind such transformations [15,16] is imbalance in the drag forces, with the drag being tied to foam films here (see e.g. the form of the drag term on an element of foam film as given within the electronic supplementary material, equation (S1.1)). As a result, the side of the structure near the upper channel wall, which has more films (as per figure 1*c*), experiences more drag than the side near the lower channel wall with fewer films. Increasing the driving pressure increases the drag overall, but also increases the imbalance in the drag. Eventually the imbalance can become unsustainable, leading to $T1$.

However, Torres-Ulloa & Grassia [15,16] found for the three-bubble system that various different types of topological transformation are now permitted: see the electronic supplementary material, section S2(b) and especially figure S2 for details of the transformation types. These include not just the so-called $T1_c$ (a vertex–vertex collision as previously seen by Drenckhan *et al.* [14] in a curved U-bend channel rather than the straight channel considered here), and the so-called $T1_u$ (a vertex reaching the upper channel wall [19], which can occur for the so-called simple lens in figure 1*a*), but also other transformation types as well. In particular, a $T1_l$ and a variant thereof a $T1_{l'}$ (both involving a vertex reaching the lower channel wall) could occur (see the electronic supplementary material, sections S3 and S4, for instances in which this happened). The various topological types are shown in the previously mentioned electronic supplementary material, figure S2. Which $T1$ type actually occurs was shown to be sensitive to the set of bubble sizes chosen relative to channel size.

For other choices of bubbles sizes, however, both methodologies (steady and unsteady state), have found that the three-bubble system could avoid $T1$ altogether and reach instead, in the limit of high imposed driving pressures, a so-called geometrically invariant state [15,16]. In this state, bubble shapes cease to change, and the structure simply moves faster and faster as the imposed back pressure keeps increasing (see sections S3 and S4 in the electronic supplementary material). This behaviour (avoiding $T1$ altogether) is akin to what commonly happens in the

infinite staircase (figure 1*b*). However, situations like these turn out to be of limited interest in the present work, which deals with topological transformation paths (i.e. the sequences of topological transformations that various three-bubble systems follow). If there is no topological transformation at all, there is likewise no transformation path. For the three-bubble system moreover, topological transformations are avoided for only a rather limited domain of bubble sizes (see the electronic supplementary material, figure S3, and also [15]). It is more common for the three-bubble system to undergo $T1$, although various different types of $T1$ could occur as already noted. In each case, which outcome the system reaches depends on the size of the bubbles, and also on the pressure imposed.

Given that both the simple lens system (figure 1*a*) and the three-bubble system (figure 1*c*) can exhibit topological transformation, in [16], the simple lens and the three-bubble system were compared to identify which of them is more resilient to $T1$. This was a delicate balance, because on the one hand, the three-bubble system is susceptible to certain $T1$ types (e.g. the $T1_c$, $T1_l$ or $T1_{l'}$ mentioned above) that the simple lens never experiences [19]. On the other hand, the three-bubble system could, again as mentioned above, sometimes reach a geometrically invariant state (resisting $T1$ altogether). What was found by Torres-Ulloa & Grassia [16] is that the simple lens tends to be more resilient for small bubble sizes (relative to channel size), but the three-bubble system is more resilient as bubble sizes increase.

Notwithstanding the comparative susceptibility or resilience to $T1$, one significant difference between the simple lens and the three-bubble system is, however, that the simple lens can only ever undergo a single $T1$, not a sequence of multiple $T1$s. This is because the structure itself in figure 1*a* is so simple, consisting just of a so-called lens bubble at the upper channel wall, and a so-called spanning film connecting that bubble to the lower channel wall. In the work of Green *et al.* [19], in cases when the simple lens structure was observed to break up, this was due to the spanning film running ahead of and separating from the lens bubble. Once that has happened no further transformations can occur. Meanwhile the three-bubble system (akin to the system studied by Drenckhan *et al.* [14], namely flow of a bubble train through a U-bend) can potentially undergo a sequence of transformations. The nature of multiple topological transformations for the three-bubble system remains an open question as is discussed next.

(b) Open questions for the three-bubble system

The steady state solution methodology of Torres-Ulloa & Grassia [15] is only designed to track steadily propagating solutions for the three-bubble system in a specified topology up to an imposed pressure corresponding to a first topological transformation: it does not interrogate what happens beyond that. Once the topology changes after a first topological transformation, the method would need to change likewise. Moreover it is not even clear that the topology obtained after a first topological transformation would necessarily admit a steadily propagating state at the imposed pressure in question. If the new topology immediately after the first topological transformation is more resilient to $T1$ than the original topology shown in figure 1*c* was, then it is likely that a steadily propagating solution will still be available at the given imposed pressure. However, if the new topology is less resilient than the original, then a steadily propagating state might not be admitted, and the steady state approach is then of little use.

The unsteady state or dynamic simulation methodology of Torres-Ulloa & Grassia [16] meanwhile can in principle track the system beyond a first topological transformation. However, Torres-Ulloa & Grassia [16] chose to stop simulating after a first transformation. The state reached after a first topological transformation as found by Torres-Ulloa & Grassia [16] might, however, be merely a short-lived intermediate state that continues to break up via a sequence of further transformations. Hence it becomes relevant to consider the entire topological transformation path that the three-bubble system follows, not just the first transformation. This then is what the present paper addresses.

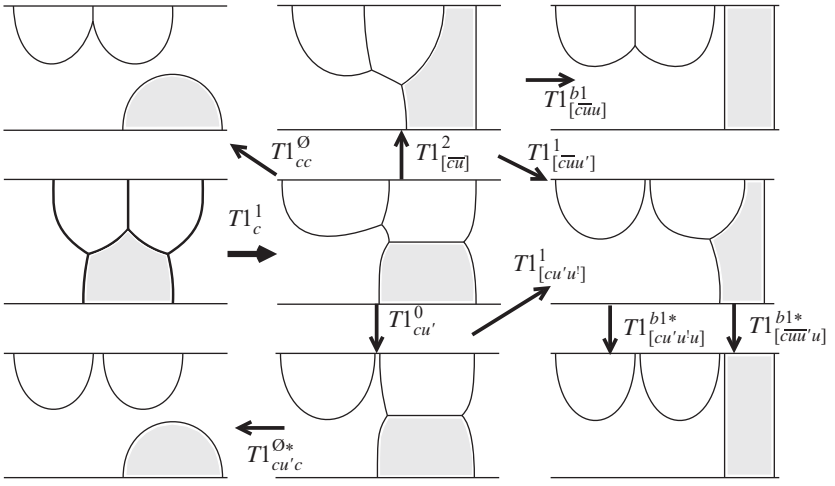

Figure 2. Topological transformation paths for systems that undergo a $T1_c$ initially starting from the original three-bubble topology. The meanings of all the various superscripts and subscripts in the diagram are explained in §3a and in more detail in the electronic supplementary material, section S6. The initial staircase topology is on the left (in bold face) and starting from there, arrows can be followed to construct the various different topological paths that are realized. Bubble $\mathcal{B}_2$ is shown shaded to distinguish it from the others.

What we will demonstrate is that the three-bubble system if it undergoes topological transformation at all, typically undergoes a sequence of transformations. After these transformations, the system reaches one of a set of what we will call final topological states. These constitute just a subset of the total set of topologies available to the three-bubble system. As we will see, these final states, unlike the state in figure 1*c*, are characterized by their topological symmetry: the number of films attached to the upper channel wall matches the number of films attached to the lower channel wall, at least in those parts of the structure that continue to propagate. As also happened with the simple lens [19] (sketched in figure 1*a*; see also section S1 in the electronic supplementary material for a brief discussion of the simple lens), when topological transformations occur, certain films might belong to bubbles that are left behind and no longer propagate (on the basis that they no longer form structures that span the entire channel). Those films are excluded from the topological symmetry count.

The focus of the present work then, as we have said, is on topological transformation paths (see figures 2–6, which also will be explained in detail later). As Torres-Ulloa & Grassia [15,16] found, the main factor determining which type of topological transformation is selected first (and hence, in turn, which transformation path is selected) is the set of bubble sizes. However, as Torres-Ulloa & Grassia [16] found, the value of the imposed driving pressure also plays a role. It is obvious of course that imposed pressure must play some role because, as has been alluded to above, $T1$ topological transformations only ever occur in the first place when driving pressure is sufficiently high. Given that, as already alluded to, the focus here is on topological transformation paths, the driving pressure needs to be high enough to induce at least one transformation.

However, the behaviour with respect to pressure is more subtle than just described. It was found by Torres-Ulloa & Grassia [16], that, given a specified set of bubble sizes, the type of first topological transformation that a three-bubble system undergoes might be sensitive to the imposed back pressure driving it. So for example, a $T1_u$ might be selected as the first topological transformation for one domain of imposed pressures, but a $T1_c$ might be selected for a different domain of pressures. Different imposed back pressures for a given set of bubble sizes can, therefore, lead to different topological transformation paths.

This then raises a number of interesting questions. The first topological transformation that is selected is evidently sensitive to pressure, but if the entire transformation path is now

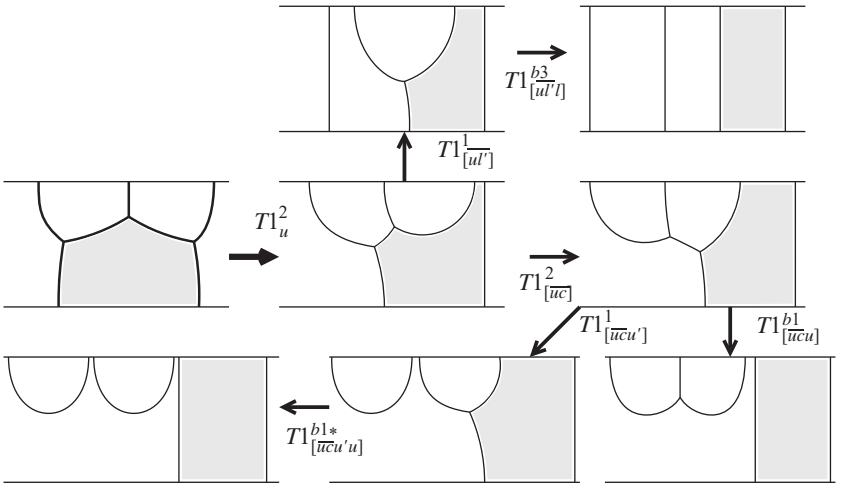

Figure 3. Topological transformation paths for system that undergo a $T1_u$ initially starting from the original topology.

considered, is it ever the case that the same set of transformations might occur, merely in a different sequence? In other words, to what extent do the various transformation types commute within a transformation path? Given also that, as has been mentioned, systems tend to reach one of just a small set of final topological states, does changing imposed pressure and thereby switching the first topological transformation type, lead the system (once the full transformation path is considered) back into the same final topological state as before? Alternatively, does switching the first transformation type in this fashion cause the system to branch onto an entirely different transformation path, leading then to a quite distinct final state? Moreover, is it possible to see second or subsequent transformations switching type as imposed pressure changes, even though the first transformation type might not change so readily? These then are questions to be addressed in the present work. The strategy for addressing these questions is described next.

(c) Simulation strategy

As alluded to earlier, the model of choice (see the electronic supplementary material, section S1) is the viscous froth model, which balances pressure, surface tension/curvature and viscous drag forces [21], the drag forces being essential for systems that depart from equilibrium. For simplicity, surface tensions are assumed to be uniform along films and constant over time here, but this assumption can in principle be changed to include surfactant effects in models [22–24]. The viscous froth model as used here is cast in a suitable dimensionless form (again see the electronic supplementary material, section S1). For each film element we find (see the electronic supplementary material, equation (S1.2))

$$v_\perp = \Delta p - \kappa, \tag{2.1}$$

where $v_\perp$ is the dimensionless velocity of a film element, Δp is the dimensionless pressure difference across the film and κ is the dimensionless curvature of a film element.

The methodology used in this work to compute unsteady state simulation for the viscous froth model is based on work developed in [19] for the simple lens, and was used in [16] for the three-bubble system to obtain results for system evolution up to the first $T1$ (see section S4 in the supplementary material for a summary of those results). The same methodology is now applied in this work to capture the dynamics of the three-bubble system as it evolves beyond the first $T1$. A brief description of the method is given in section S5 in the electronic supplementary material. Essentially what is involved here is sudden imposition of a driving back pressure p_b to

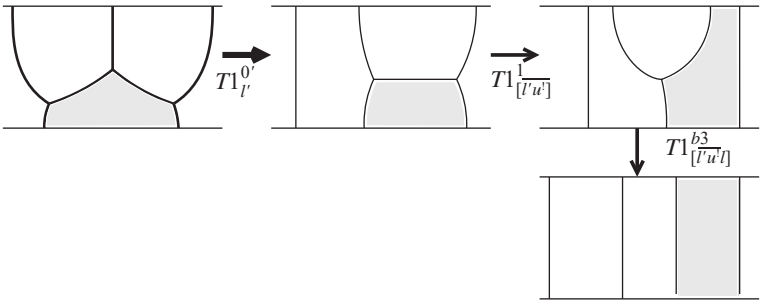

Figure 4. Topological transformation paths for systems that undergo a $T1_{l'}$ initially starting from the original topology.

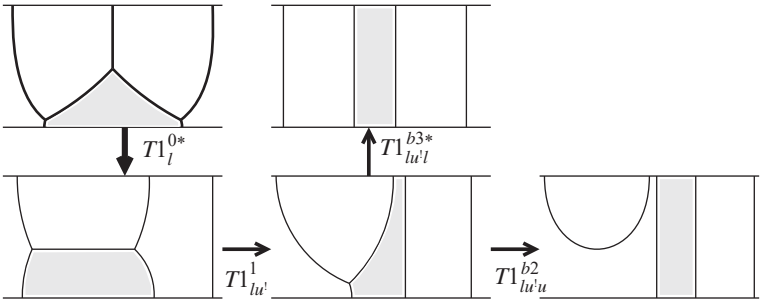

Figure 5. Topological transformation paths for systems that undergo a $T1_{l}$ initially starting from the original topology.

set the three-bubble system into motion. Thus p_b is reset from zero to some specified non-zero value, and held at that value. As a result, the foam films move, and some of them tend to grow while others tend to shrink. If any film shrinks below a critical cut-off value (see the electronic supplementary material, S5(b) for details), a topological transformation is declared.

Assuming the imposed pressure is high enough to induce a first topological transformation, then the simulation technique should have no difficulty continuing beyond that first transformation. In principle topological transformations must continue until the system finds itself in a topological configuration that is sufficiently strong to resist them. Indeed, for a given (dimensionless) imposed back pressure p_b, the (dimensionless) apparent velocity v at which film elements seem to migrate along the channel need not be spatially uniform over the entire structure, at least not until (as already discussed in §2a) a steadily propagating structure is reached.

Note also that a so-called bamboo configuration, with films on individual bubbles spanning the entire channel from the upper to the lower channel wall [15] (see figures 3–5 for examples), can propagate steadily without breaking even with arbitrarily large imposed pressures. Variants of the bamboo configuration also admit bubbles that are left behind attached to one or other channel wall, while the remaining films propagate steadily as a bamboo (see figures 2, 3 and 5 for examples). Hence a bamboo is a conceivable final configuration for a system after multiple topological transformations, albeit not necessarily the only possibility, as we will see.

To summarize, by computing unsteady state simulation, our strategy is to determine how systems will evolve after their first topological transformation, tracking the evolution until they reach a steadily migrating configuration for the specified imposed back pressure: a system might typically undergo a sequence of different topological transformations before reaching such a state (see §3 for details). Dealing with multiple topological transformations, rather than just a single transformation, is then the key novel aspect in what follows.

3. Multiple transformations: identifying permitted paths

As mentioned in §2a and as also detailed in section S2(b) in the electronic supplementary material, the first topological transformation that the system can undergo can be of four distinct types (see figure S2 in the electronic supplementary material): $T1_c$ (vertex–vertex collision), $T1_u$ (transformation at the upper channel wall at the downstream end of the structure), $T1_l$ (transformation at the lower channel wall at the downstream end of the structure) and $T1_{l'}$ (like $T1_l$ but happening further upstream). When considering subsequent transformations within a sequence of multiple transformations, however, yet another transformation type also becomes common, namely the $T1_{u'}$ (like $T1_u$ but happening further upstream): see figures 2 and 3 for some examples involving the $T1_{u'}$.

The type of first topological transformation and the types of any subsequent topological transformations selected depend on bubble sizes and also upon the different back pressures that are imposed. To interrogate this, we have generated a large body of simulation results (see section S8 in the electronic supplementary material). Before we can consider the results in detail (which we do in §4), we need a notation to describe the various topological transformation paths as predicted by our simulations. In what follows, therefore, the different paths will be identified based on the historical sequence of topological configurations that the system is observed to undergo.

(a) Designating topological paths and topological states

The notation we employ for topological transformation paths is consistent with the notation already established above and in the electronic supplementary material, section S2(b), for the first topological transformation. Specifically an individual topological transformation in the historical sequence of transformations will be denoted with the subscript c if it involves a collision of vertices, by the subscript u if the vertex furthest downstream reaches the upper channel wall, and by the subscript l if the vertex furthest downstream reaches the lower channel wall. If, on the other hand, a vertex further upstream reaches either the upper or the lower channel wall, the topological transformation will be specified with the subscript u' or l', respectively. Therefore, the topological path of systems that have undergone more than one different topological transformation could be denoted as e.g. $T1_{cu'uu}$ or $T1_{l'ul}$.

Figures 2–5 (as discussed in detail in §3b to follow) sketch the possible topological transformation paths, with an overall summary in figure 6. All the paths shown in these figures are actually observed for at least some choices of bubble sizes and some choices of imposed driving pressure. Transformations that are topologically feasible but never actually observed dynamically via the simulation methodology (the methodology itself is described in section S5 in the electronic supplementary material) are not shown here. For example the dynamics would not typically favour transformations that involve bubbles near the upper channel wall (where there are more films and hence more viscous drag) running increasingly far ahead of and overtaking bubbles near the lower channel (fewer films and less drag). In summary, figures 2–6 include only those transformations that the dynamics actually manages to select.

Over and above what is shown in §3b below, we have extended the discussion of multiple topological transformations as follows (details are relegated to the electronic supplementary material, section S6: some readers may find it helpful to consult that section immediately). When systems undergo more than one topological transformation we use a special notation to identify configurations that are topologically equivalent, despite possibly being reached by different paths (see section S6(a) in the electronic supplementary material for details). Briefly, however, a square bracket around the subscript in figures 2–6 indicates a path that is topologically equivalent to at least one other path. In addition, an overbar on the first two transformations in the path indicates they are topologically interchangeable. Understanding that various different topological paths commute also helps us to draw a clearer distinction between the concept of a 'topological path'

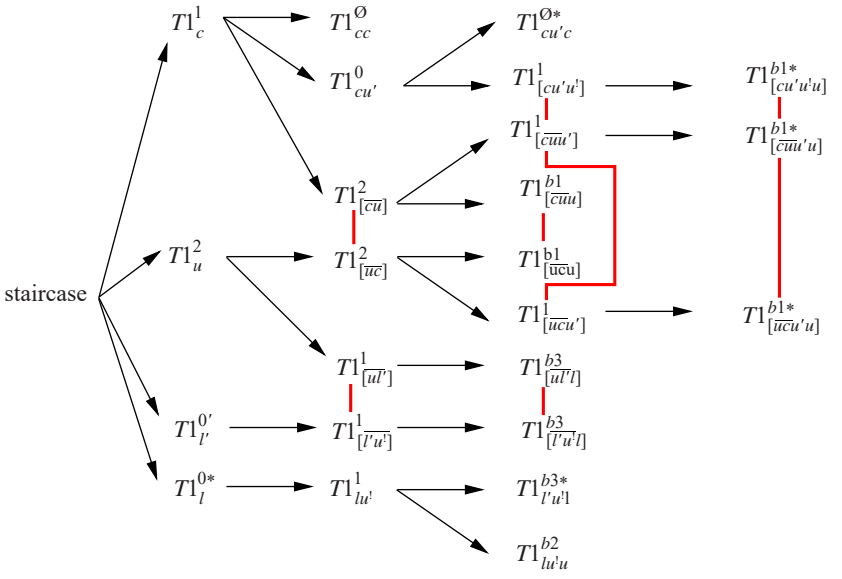

Figure 6. Full set of topological transformation paths observed for the three-bubble system starting from a staircase structure. Remember that it is not necessary to follow each path to the end. Topologically equivalent states reached by different paths are shown connected vertically by lines: for more information see also figure S14 right at the end of the electronic supplementary material.

and the concept of a 'topological state'. As we explain further in the electronic supplementary material, section S6(a), a topological state is the topology that results when a particular topological path is followed. The path defines the state, but not *vice versa*, since a given state might be reached by various different paths.

Clearly the subscript notation we have defined thus far pertains to paths. Our aim, therefore, in what follows is to augment that notation using superscripts to designate particular states. Both subscripts and superscripts, therefore, appear in figures 2–6 (see §3b). The advantage of augmenting the notation in this fashion is that we can then use a common notation interchangeably to represent either 'topological paths' or 'topological states' depending on which concept is being discussed.

Towards that end, we identify a number of topological final states which by their nature typically manage to avoid undergoing any further transformations. These final states can be divided into two types: so-called 'endpoint states', which cannot undergo any further transformations whatsoever, and so-called 'metastable states', which resist breaking, but which can still be broken in principle. As will become apparent, much of what follows focuses on final states like these.

(Details of some endpoint states can be found in sections S6(b)–S6(c) in the electronic supplementary material). In this context, the superscript Ø and a variant thereof Ø∗ will be used to indicate systems that break up completely and cease to propagate (examples can be found in figure 2). The superscripts $b3$, $b2$ and $b1$ meanwhile indicate bamboo states (mentioned already in §2c), with either three bubbles, two bubbles or one bubble still moving. Variants $b3*$ and $b1*$ also exist. These bamboo states (see various examples in figures 2–6), once formed will propagate but can never be broken.

Moving on to consider topological states more generally (not just endpoint states), properties that various states have that might help them either to avoid further topological transformations or be particularly susceptible to them are discussed in sections S6(d)–S6(g) in the electronic supplementary material. One useful measure here is a topological asymmetry index (see section S6(d) and also section S6(f) in the electronic supplementary material), which is simply the

difference between the number of films attaching to the upper channel wall and the lower channel wall, but counting only those films that actually propagate. Where relevant, i.e. with the exception of endpoint states which already have their own bespoke superscripts as mentioned above, the value of the asymmetry index is shown as a superscript in figures 2–6.

It turns out that states with non-zero asymmetry index are often rather short-lived, so it is instead the states that are symmetric topologically speaking (i.e. having zero asymmetry index) which are deemed as being of particular importance. The bamboo states are themselves topologically symmetric, but there are other topologically symmetric states as well, as section S6(e) in the electronic supplementary material describes. These are identified also in figures 2, 4 and 5 shown with a superscript 0 (or variants thereof $0'$, $0*$). We also refer to these particular states as 'two-bubble' states because they involve two bubbles stacked across the channel, with a third bubble either upstream or downstream but not impacting on how the other two bubbles are configured. Such states are difficult to break, meaning they are selected very often as final states. Electronic supplementary material, section S6(e), designates the 0, $0'$ and $0*$ states as 'metastable', a terminology already alluded to above, which will be employed also in what follows. Even though these states often resist breaking, they can still be broken under certain circumstances, although the particular circumstances causing them to break may need to be analysed carefully (for more information see the electronic supplementary material, section S7 and in particular section S7(b)). Transformation paths (themselves denoted by subscripts) which involve breaking metastable states are designated as 'counterintuitive' (see the electronic supplementary material, sections S6(e) and S7(b) for details) and, where relevant, in figures 2, 4 and 5 a superscript '!' is placed upon the already existing subscript to highlight them. The superscript '!' is placed at the specific step in the path which breaks the metastable state.

This then completes a description of the notation deployed in figures 2–6 (further details being found in the electronic supplementary material, section S6), so now we can proceed to present the figures themselves in §3b below. An overall summary of all the discussion here is then offered in §3c.

(b) Diagrams of topological transformation paths

Here we sketch diagrammatically all the possible topological transformation paths that the three-bubble system has been observed in simulations to undergo starting initially from the original staircase configuration (i.e. starting from equilibrium) with a range of bubble sizes, and then imposing a wide range of driving back pressures (see also analysis of particular paths in section S7 plus a full dataset in section S8 in the electronic supplementary material). As mentioned, there are some transformations that are topologically feasible, but which have not been observed (being dynamically unfavourable), and they are specifically not described here. We show the paths broken down into four different types of initial $T1$s (see figure S2 in the electronic supplementary material for the initial $T1$s and see also figures 2–5 for the resulting paths). Specifically, in figure 2 we show the possible paths for systems that start with $T1_c$, in figure 3 those starting with $T1_u$, in figure 4 those starting with a $T1_{l'}$, and finally in figure 5 those starting with $T1_l$. The full set of paths is summarized in figure 6: see also figure S14 on the landscape format page right at the end of the electronic supplementary material.

In each case, systems can undergo up to three or four transformations in the path depending on the initial $T1$ type. However, not all transformation paths involve that many transformations. Often (as we will see later on) systems follow a path involving just one or two transformations, not three or four of them.

An example of how to read figure 2 is given below, with figures 3–5 being read in a similar fashion. In figure 2, we start in the initial staircase topology (see the state indicated with bold lines towards the left), then we follow an arrow to the right ($T1^1_c$). After that we could choose, for instance to follow an arrow downward ($T1^0_{cu'}$). A possible next step would then be to follow an arrow upward and to the right ($T1^1_{[cu'u^!]}$), and from there to follow another arrow downward

Table 1. Number of instances of topological transformation paths of each type for different imposed back pressure p_b. For each p_b, we consider $l_1^\circ \in [0.1, 0.2, \ldots, 0.9, 0.96]$ and $l_2^\circ/l_1^\circ \in [0.1, 0.2, \ldots, 0.9]$ (i.e. 90 cases in total). Note that $T1_{cc}^{\varnothing}$ (figure 2) and $T1_{lu^{\prime}u}^{b2}$ (figure 5) states are allowed paths also, however, not for the specific pressures shown here. Additionally, note also that there is another way of reaching the $b1*$ bamboo state, namely $T1_{[cu^{\prime}u^{\prime}u]}^{b1*}$ (figure 2), although again not seen for the specific pressures here. Full datasets are in section S8 in the electronic supplementary material. Note moreover that $\times$ here means no $T1$.

$T1\backslash p_b$	10	20	40	80
$T1_{cu^{\prime}c}^{\varnothing*}$	0	1	2	3
$T1_{[\overline{cu}u]}^{b1}$	0	1	1	0
$T1_{[\overline{uc}u]}^{b1}$	31	28	21	14
$T1_{[\overline{cu}u^{\prime}u]}^{b1*}$	0	1	2	0
$T1_{[\overline{uc}u^{\prime}u]}^{b1*}$	0	2	5	8
$T1_{[\overline{ul^{\prime}l}]}^{b3}$	1	0	0	0
$T1_{[\overline{l^{\prime}u^{\prime}l}]}^{b3}$	1	0	0	0
$T1_{lu^{\prime}l}^{b3*}$	1	2	2	0
$T1_{l^{\prime}}^{0^{\prime}}$	0	0	0	2
$T1_{l}^{0*}$	6	7	7	1
$T1_{cu^{\prime}}^{0}$	3	28	43	56
$\times$	47	20	7	6
total	90	90	90	90

($T1_{[cu^{\prime}u^{\prime}u]}^{b1*}$). If instead, from the $T1_c^1$ state, we were to follow an arrow upward we would reach $T1_{[\overline{cu}]}^2$. Selecting an arrow downward and to the right would lead to $T1_{[\overline{cu}u^{\prime}]}^1$ (equivalent to $T1_{[cu^{\prime}u^{\prime}]}^1$ but reached by a different path). A downward arrow now leads to $T1_{[\overline{cu}u^{\prime}u]}^{b1*}$ (likewise equivalent $T1_{[cu^{\prime}u^{\prime}u]}^{b1*}$ but reached by a different path). In any case, following all the various arrows in each of figures 2–5 it is possible to construct the full set of possible paths and possible states that are observed, summarized in figure 6. It should be remembered, however, that it is not necessary for paths to follow all arrows shown all the way to the end. In the example described above for instance, the topology might well stop evolving upon reaching $T1_{cu^{\prime}}^0$ for instance, rather than necessarily continuing on to $T1_{[cu^{\prime}u^{\prime}]}^1$ or $T1_{[cu^{\prime}u^{\prime}u]}^{b1*}$.

(c) Summary of topological paths and states

This now completes the designation (via subscript notation) and diagrammatic representation of the various topological paths that systems are observed to take, based on our simulation results. We have also identified (via superscript notation) the topological states that the various paths access. Further detailed discussion of topological paths and topological states is given in section S6 in the electronic supplementary material. A key point, however, is that out of the many different states that systems access in the diagrams while following their topological paths, only a subset of them are expected to be final states with the system then propagating steadily without further topological transformations occurring (further details of which states simulations actually select as final states can be found in table 1 which is discussed further later on; typically topologically symmetric states are favoured as final states).

Unsteady state simulation results are now analysed to explore not just the sets of topological transformation paths that systems follow, but also how often they are followed. Likewise the analysis tells us not just the sets of final states that systems reach, but also how often they are reached. The complete details for all the cases studied in this work are summarized in section S8 in the electronic supplementary material, covering a wide domain of bubble sizes and imposed back pressures, i.e. a wide domain of l_1°, l_2°/l_1° and p_b values. An illustration of the behaviour in just a selection of these cases is presented next in §4.

4. Results and discussion

We now proceed to present simulation results for specific imposed back pressures and for values of $l_1^\circ \in [0.1, 0.2, \ldots, 0.9, 0.96]$ and $l_2^\circ/l_1^\circ \in [0.1, 0.2, \ldots, 0.9]$. As in [16], the rationale for choosing $l_1^\circ = 0.96$ in particular is that it accesses some states that the other l_1° values considered do not reach. Section 4a focuses on results in detail for just a small selection of imposed pressures. Section 4b meanwhile focuses on many more imposed pressures but looks at information from a more statistical point of view. Finally §4c considers the mobility of various states that result. Further information helping to explain the system behaviour in detail is discussed in section S7 in the electronic supplementary material. Moreover, although the focus throughout is on topology and to a lesser extent on mobility, it is also instructive to consider system energy, which is done in section S9 in the electronic supplementary material.

(a) Topological transformation paths for a selection of pressures

In figures 7–10, we indicate the various topological transformation paths that are seen for different imposed back pressures $p_b \in [10, 20, 40, 80]$, recalling that pressures here are taken to be dimensionless on a scale associated with capillary effects (see the electronic supplementary material, section S1, for details of how the system is made dimensionless; the same approach was used by Torres-Ulloa & Grassia [15,16], and the domain of dimensionless pressures explored was comparable with the domain that is considered here). Data presented in figures 7–10 are expressed in the form of phase diagrams, namely the topological path followed in each case at each pressure p_b as a function of l_1° and l_2°/l_1°. Remember here (see section S2 in the electronic supplementary material) that, with the distance between upper and lower walls scaled to unity, varying l_1° and l_2°/l_1° just corresponds to varying bubble areas. The notation on the phase diagram matches the superscript and subscript notation already defined in §3, although the symbol $T1$ is omitted in the diagram itself in order to save space. A summary of the different $T1$ paths for each p_b considered is given in table 1.

Here, as we have said, we present an illustration of the possible outcomes for just four distinct p_b values. However, other paths can also be followed, if values of p_b different from those in figures 7–10 are considered. This is detailed in section S8 in the electronic supplementary material. For the four distinct p_b values to be considered here though, we start in §4a(i) with an overview of the paths followed, then §4a(ii)–(iv) give the paths for each of the pressures. After that, §4a(v)–(vi) give populations of states for each path, and populations transitioning between paths.

(i) Overview of topological transformation paths

Before we proceed there is a notational convention that we clarify in order to facilitate the discussion. A topological path involving multiple steps, or indeed multiple steps that occur towards the start of a given topological path, will be denoted by multiple subscripts plus a superscript: that notation has been defined already in §3. Meanwhile the first step in a topological path (the path itself might or might not involve multiple steps) will be denoted with a single subscript plus a superscript, e.g. $T1_c^1$, $T1_u^2$, $T1_l^{0*}$ or $T1_{l'}^{0'}$. The symbols $T1_c$, $T1_u$, $T1_l$ or $T1_{l'}$ or indeed $T1_{u'}$ (without a superscript) meanwhile denote generic transformation types, which might occur as the first step in a path, but which might instead occur as a subsequent step. These generic

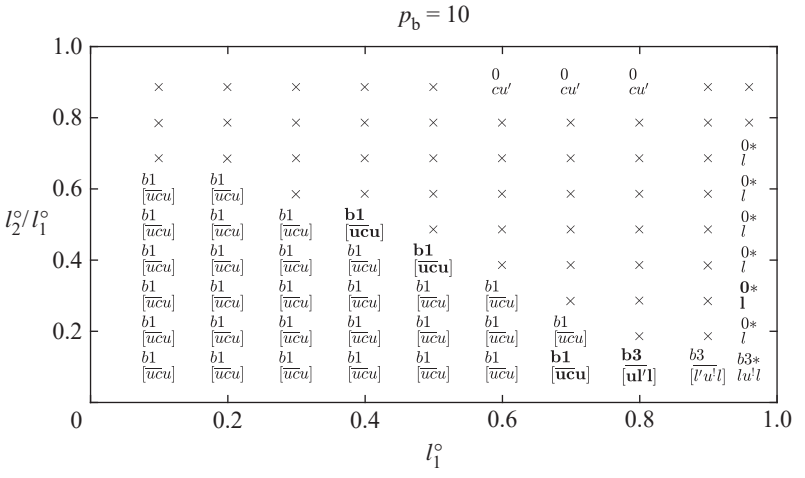

Figure 7. Topological transformation paths for values of $l_1^\circ \in [0.1, 0.2, \ldots, 0.9, 0.96]$, and $l_2^\circ/l_1^\circ \in [0.1, 0.2, \ldots, 0.9]$, in each case with $p_b = 10$. Topological states are also indicated along with the paths. Cases shown in bold are in buffer regions in which it is already known that different transformation types compete (see section S3(b) in the electronic supplementary material).

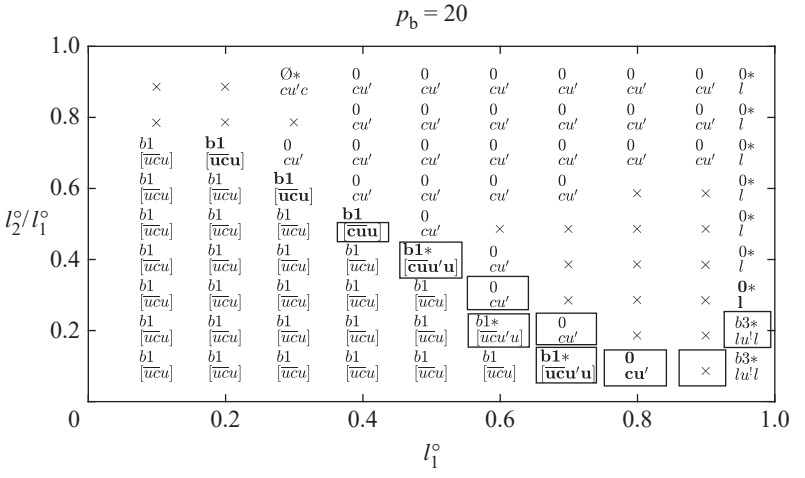

Figure 8. Topological transformation paths and topological states for values of $l_1^\circ \in [0.1, 0.2, \ldots, 0.9, 0.96]$, and $l_2^\circ/l_1^\circ \in [0.1, 0.2, \ldots, 0.9]$, in each case with $p_b = 20$. Cases shown in bold are in buffer regions in which different *T*1 types are known to compete. Cases enclosed in a box are those which differ between the present pressure $p_b = 20$ and the pressure $p_b = 10$ in the previous figure, albeit excluding situations for which $p_b = 10$ did not exhibit any *T*1 at all. The box is drawn just around the transformation path, if a different transformation path results in the same final outcome, i.e. the same topological state. Otherwise the box is drawn around both the path and the state.

transformation types do not carry a superscript, because the superscript required depends on the topological state, which cannot be specified unless we know the full sequence of transformations up to and including any given point in a given path.

An important observation we make from figures 7–10 is that the overwhelming majority of the cases considered that manage to undergo topological transformations at all, end up propagating in states with a topological asymmetry index of zero, implying equal numbers of propagating films attaching to upper and lower channel walls. There are a few cases in which systems break up in a fashion such that no films propagate at all: these are denoted Ø or Ø∗ (see also figure 2), and they have themselves been discussed in sections S6(b) and S7(a) in the electronic supplementary

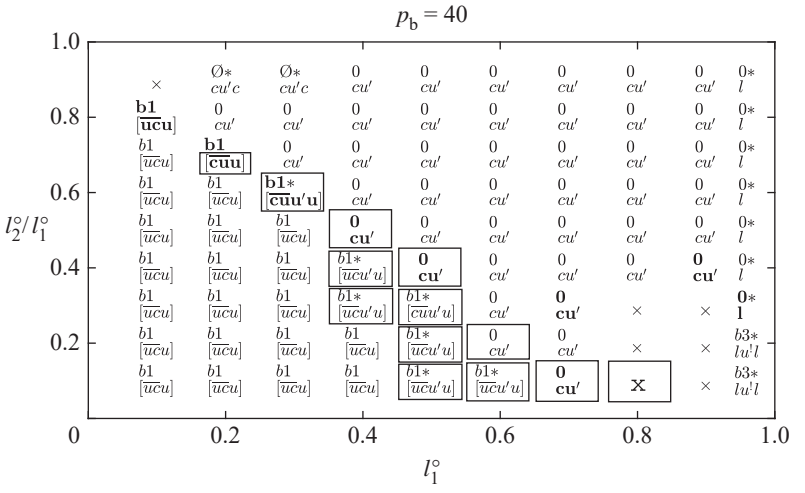

Figure 9. Topological transformation paths and topological states for values of $l_1^\circ \in [0.1, 0.2, \ldots, 0.9, 0.96]$, and $l_2^\circ/l_1^\circ \in [0.1, 0.2, \ldots, 0.9]$, in each case with $p_b = 40$.

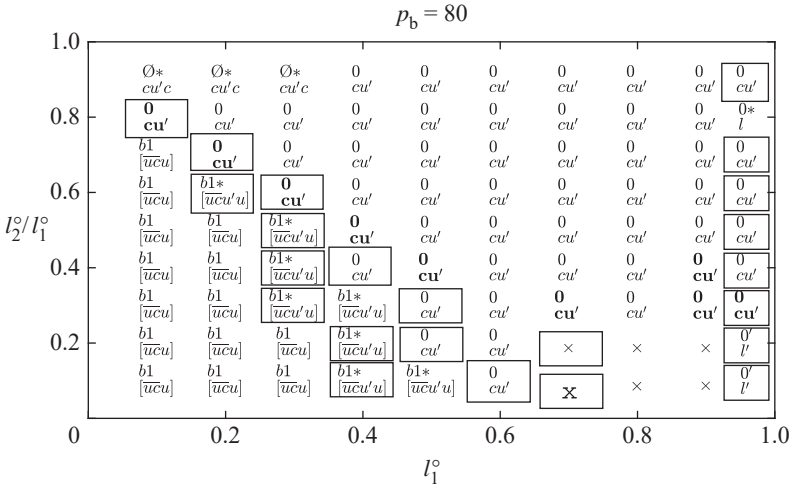

Figure 10. Topological transformation paths and topological states for values of $l_1^\circ \in [0.1, 0.2, \ldots, 0.9, 0.96]$, and $l_2^\circ/l_1^\circ \in [0.1, 0.2, \ldots, 0.9]$, in each case with $p_b = 80$.

material. Overall, however, it is clear from figures 7 to 10 that three-bubble systems have a strong preference for selecting propagating states that are topologically symmetric. This includes systems that finish in a bamboo-like configuration, labelled as $b1$ and $b3$ (or variants thereof $b1*$ or $b3*$). These are topological endpoint states permitting films to propagate under any imposed driving pressure without any film deformation at all, and hence without any possibility of further topological change (see section S6(c) in the electronic supplementary material). Not all the symmetric states selected are, however, topological endpoint states: often systems select metastable states instead such as $T1^{0}_{cu'}$, $T1^{0'}_{l'}$ or $T1^{0*}_{l}$. These are all topologically symmetric (see figures 2, 4 and 5 for how they are configured), and so (as section S6(e) in the electronic supplementary material describes) tend to resist breakage in practice, even though in principle they could still be broken.

The fact that, if systems undergo topological transformation at all, then they eventually find themselves in states with zero asymmetry index, implies that all the (asymmetric) intermediate

states that systems pass through on their way to an eventual (symmetric) state, are presumably less resilient than the original three-bubble staircase configuration was. In other words, even though the original three-bubble state is not entirely resilient to $T1$ and can be broken, it is typically more resilient than any asymmetric daughter states that derive from it, e.g. $T1^2_u$ or $T1^1_c$ on their own, or else combinations of them such as $T1^2_{[\overline{uc}]}$, $T1^1_{[\overline{uc}u']}$, $T1^2_{[\overline{cu}]}$, $T1^1_{[\overline{cu}u']}$, all of which within figures 7–10 always break further. If we look moreover at a much bigger sample of data (see tables S1–S10 in section S8 in the electronic supplementary material, including many more imposed pressures than are analysed in figures 7–10, specifically incrementing pressure in integer steps) we see a few isolated cases of systems remaining in asymmetric states ($T1^2_u$, $T1^2_{[\overline{uc}]}$, $T1^1_{[\overline{ul'}]}$ in particular). However, this turns out to occur in very restricted domains of bubble sizes l_1°, l_2°/l_1° and driving pressures p_b. The overwhelming preference for evolving into topologically symmetric states is clear.

In the steady state approach of Torres-Ulloa & Grassia [15], regions of parameter space which are firmly $T1^1_c$, $T1^2_u$, $T1^{0*}_l$ or $T1^{0'}_{l'}$ (as the first $T1$ transformation) were found. However, there were also so called buffer regions between them, within which different $T1$ types compete (see section S3 in the electronic supplementary material for details, in particular section S3(b)). States within the already identified buffer regions [15] are highlighted with boldface in figures 7–10. In these buffer regions and nearby to them, it has been shown [16] (for the first $T1$ at least) that the $T1$ type predicted by unsteady state simulation often differs from the $T1$ type predicted by the steady state approach, and moreover the $T1$ type selected by the unsteady state simulation could readily switch from one type to another as p_b varied.

By the same token, and via the same unsteady state simulation approach considered here, transitions between entire topological transformation paths are possible just by varying p_b. These are highlighted in boxes in figures 7–10, which adopt a subscript and superscript notation that was established in §3. More specifically a topological path is highlighted in a box in figures 8–10 if it differs from the topological path at the next pressure down in figures 7–9. A box just around the subscript alone shows a different topological path, but the final state is the same, while a box around both subscript and superscript is used if the path is different and the final state is also different.

Referring back to the various open questions posed in §2b, our data (see the electronic supplementary material, section S8, for details) now permit us to address many of them. There are for instance cases in which for a given l_1° and l_2°/l_1°, different p_b values eventually lead the system to the same final state but via different routes. Such a case is $l_1^\circ = 0.3$ and $l_2^\circ/l_1^\circ = 0.6$ (see the electronic supplementary material, table S3), which has no $T1$ up to $p_b = 11$ (consistent with figure 7 for $l_1^\circ = 0.3$ and $l_2^\circ/l_1^\circ = 0.6$), undergoes $T1^{b1}_{[\overline{uc}u]}$ for $p_b \in [12, \ldots, 24]$ (consistent with figure 8), but $T1^{b1}_{[\overline{cu}u]}$ for $p_b \in [25, \ldots, 31]$. Changing driving pressure, therefore, leads in this instance to the same state reached via different paths. Beyond that, however, changing pressure causes this system to branch to a different final outcome, i.e. $T1^{b1*}_{[\overline{cu}u'u]}$ for $p_b \in [32, \ldots, 44]$ (which is evident from figure 9). Reaching this different outcome has resulted from a change in the third transformation in the path, keeping the first two intact. This same outcome is reached again (but via a different path $T1^{b1*}_{[cu'u'u]}$) for $p_b \in [45, \ldots, 49]$: the change is now seen from the second transformation in the path. Meanwhile for $p_b \in [50, \ldots, 80]$, the outcome is different yet again, namely $T1^0_{cu'}$ (which is evident from figure 10). Details of behaviours such as these are given in tables S1–S10 in the electronic supplementary material for pressures up to $p_b = 80$ in integer steps. In the sections that follow, however, we focus specifically, as we have said, just on selected p_b values $p_b \in [10, 20, 40, 80]$, and how systems behave for those particular pressures. Note also that previous work [15,16] has found that $p_b = 80$ often tends to be sufficient for large p_b limiting behaviours to emerge.

(ii) Topological transformation paths for $p_b = 10$

In figure 7 (for $p_b = 10$), we can see that for small values of l_1° and l_2°/l_1° (bottom left region of the phase diagram), systems undergo $T1^{b1}_{[\overline{uc}u]}$, where bubbles $\mathcal{B}_1$ and $\mathcal{B}_3$ are left behind (attached

together), while bubble $\mathcal{B}_2$ keeps flowing in a bamboo configuration (see figure 3 for a sketch of the path followed). In this region of the phase diagram, it turns out [15] that geometrically bubble $\mathcal{B}_2$ is rather larger in area than $\mathcal{B}_1$ and $\mathcal{B}_3$, and manages to slip away from those other bubbles relatively easily.

Still with small l_1°, when bigger values of l_2°/l_1° are considered (i.e. values of l_2°/l_1° closer to unity), the system does not undergo any topological transformation, at least not for $p_b = 10$, which is as expected from Torres-Ulloa & Grassia [15]: small l_1° but large l_2°/l_1° resists the first $T1$ out to large p_b (see the electronic supplementary material, sections S3 and S4). This behaviour has been attributed [15] to the geometric placement of vertex V_3 on bubble $\mathcal{B}_3$. Despite that bubble being small in area, the vertex is placed still some distance away from the bubble's downstream edge such that it is less easy for bubble $\mathcal{B}_2$ to slip away.

As l_1° increases, $T1^{b1}_{[\overline{uc}u]}$ is still obtained for small values of l_2°/l_1° (see figure 3), but as l_2°/l_1° increases, systems stop undergoing topological transformation at least for $p_b = 10$ as is considered here. For even larger values of l_2°/l_1°, the systems undergo $T1^0_{cu'}$ in a few cases. Geometrically, these particular cases correspond to bubble $\mathcal{B}_2$ now being a little smaller in area than $\mathcal{B}_1$ and $\mathcal{B}_3$, and the topological transformation can be traced back again to vertex placement [15]: vertices V_1 and V_2 are close together and collide easily. The final result is that bubble $\mathcal{B}_1$ is left behind and bubbles $\mathcal{B}_2$ and $\mathcal{B}_3$ keep flowing attached together in a two-bubble structure spanning the channel, see figure 2. This is a topologically symmetric state: as mentioned earlier, it is a metastable state that is difficult to break. However, it is not formally an 'endpoint state' that could never be broken.

Still consulting figure 7, for yet bigger values of l_1° (e.g. $l_1^\circ \in [0.8, 0.9]$), systems resist topological transformation for a larger domain of l_2°/l_1° values, but $T1^{b3}_{[\overline{ul'}l]}$ and $T1^{b3}_{[\overline{l'u^!}l]}$ are observed for $l_2^\circ/l_1^\circ = 0.1$. These transformation paths lead to an 'endpoint state', namely a bamboo configuration with bubble $\mathcal{B}_2$ at the leading edge of the structure (figures 3 and 4). Geometrically all bubbles are of large area in this region of the phase diagram [15], so it is not surprising that a bamboo state is reached: large bubbles tend to prefer bamboo states, rather than staircase structures that zig-zag across the channel [9]. What is perhaps less obvious is how bubble $\mathcal{B}_2$ manages to overtake bubble $\mathcal{B}_3$ entirely to finish at the downstream end. The answer, however, can be traced back to the fact that l_2°/l_1° is small, meaning that the original three-bubble structure is almost at the point of breaking into two separate simple lenses. Even though it does not actually break in that particular fashion, it is still the case that the downstream film of $\mathcal{B}_2$ along with bubble $\mathcal{B}_3$ almost form a simple lens, that can evolve, at least to some extent, independently of what bubble $\mathcal{B}_1$ is doing. This is what then permits bubble $\mathcal{B}_2$ to run ahead. Further discussion of this is given in section S7(b)iii in the electronic supplementary material.

Finally for values of $l_1^\circ = 0.96$ but still with $l_2^\circ/l_1^\circ = 0.1$ we obtain neither $T1^{b3}_{[\overline{l'u^!}l]}$ nor $T1^{b3}_{[\overline{ul'}l]}$ (both bamboo structures with bubble $\mathcal{B}_2$ at the downstream end as we have mentioned). Instead the system undergoes $T1^{b3*}_{lu^!l}$ (figure 5), which corresponds to a bamboo configuration with bubble $\mathcal{B}_2$ now in the middle of the structure. Reaching a bamboo is unsurprising, since again we are dealing with large area bubbles, which often have a preference for bamboo. The reason that $T1_l$ or more specifically $T1_l^{0*}$ is selected as the first transformation is due to vertex V_3 being placed very close to the lower channel wall meaning that it can slip easily off the rest of the structure [15]. The reason why subsequent transformations occur even after that to give $T1^{b3*}_{lu^!l}$, is considered in section S7(b)ii in the electronic supplementary material. Certainly for the same $l_1^\circ = 0.96$ value, as l_2°/l_1° increases, the system undergoes just $T1_l^{0*}$ without any transformation after that: as one of the identified metastable states, this $T1_l^{0*}$ should manage to resist further transformations effectively. Meanwhile for $l_1^\circ = 0.96$ with $l_2^\circ/l_1^\circ > 0.7$ no $T1$s are observed, at least not for $p_b = 10$ considered here.

Even though we have discussed various topological transformation paths that are realized here, an important observation is that for $p_b = 10$ (the specific driving pressure considered in figure 7), many systems still manage to avoid topological transformation altogether (systems that avoid $T1$ are denoted $\times$). In figure 7, transformations are most likely to be avoided if we select intermediate to large l_1° values and intermediate to large values of l_2°/l_1°. As we will see in what follows, increasing p_b makes it increasingly difficult for $T1$ to be avoided.

A final comment we make is that when $p_b = 10$ we observed two different systems (one for $l_1^\circ = 0.8$ and $l_2^\circ/l_1^\circ = 0.1$ following a path $T1^{b3}_{[\overline{ul'}l]}$, and one for $l_1^\circ = 0.9$ and also with $l_2^\circ/l_1^\circ = 0.1$ following $T1^{b3}_{[\overline{l'u^!}l]}$) reaching a $b3$ bamboo state by different routes (see figures 3 and 4 to understand the paths followed). It turns out that there can be multiple paths to other bamboo states also. When $p_b = 20$ or $p_b = 40$ (as is studied next), very occasionally $b1$ is reached by $T1^{b1}_{[\overline{cu}u]}$ (such is the case for $l_1^\circ = 0.4$ and $l_2^\circ/l_1^\circ = 0.5$ for $p_b = 20$, and for $l_1^\circ = 0.2$ and $l_2^\circ/l_1^\circ = 0.7$ for $p_b = 40$), but far more often it is reached by $T1^{b1}_{[\overline{uc}u]}$ (see figures 2 and 3 for the paths followed). When $p_b = 20$ or $p_b = 40$, there are also different routes to $b1*$, the path $T1^{b1*}_{[\overline{cu}u'u]}$ (such as the case for $l_1^\circ = 0.5$ and $l_2^\circ/l_1^\circ = 0.4$ for $p_b = 20$, and for $l_1^\circ = 0.3$ and $l_2^\circ/l_1^\circ = 0.6$ for $p_b = 40$) being less frequent than $T1^{b1*}_{[\overline{uc}u'u]}$ (again see figures 2 and 3 to understand what the paths involve).

(iii) Topological transformation paths for $p_b = 20$

In figure 8 (for $p_b = 20$), we can see similar results to those in figure 7 (for $p_b = 10$), at least for small values of l_1°. The transformation path $T1^{b1}_{[\overline{uc}u]}$ is observed for a large domain of l_2°/l_1° values, while no $T1$s are observed for large l_2°/l_1°. As l_1° increases from small values towards intermediate values, we find some cases (see cases enclosed in a box in figure 8) in which systems have chosen different topological transformation paths with also a different final state in comparison to those chosen for $p_b = 10$. There is also a case (box enclosing just the subscript but not the superscript) for which different paths are observed but the same final state is reached.

In particular (consulting the various cases enclosed in boxes within figure 8 but focusing still on intermediate l_1° values) we see that these transitions between different paths tend to occur in the region (indicated in bold face) in which different $T1$ types are known to compete (see section S3 in the electronic supplementary material and in particular section S3(b)). One example is $T1^{b1}_{[\overline{uc}u]}$ (at $p_b = 10$) changing to $T1^{b1}_{[\overline{cu}u]}$ (topologically equivalent to $T1^{b1}_{[\overline{uc}u]}$) at $p_b = 20$. Another example is $T1^{b1}_{[\overline{uc}u]}$ (at $p_b = 10$) changing to either $T1^{b1*}_{[\overline{cu}u'u]}$ or $T1^{b1*}_{[\overline{uc}u'u]}$ at $p_b = 20$ (these $b1*$ states are topologically equivalent to each other, but not equivalent to $T1^{b1}_{[\overline{uc}u]}$). Yet another change seen is $T1^{b1}_{[\overline{uc}u]}$ (at $p_b = 10$) to $T1^{0}_{cu'}$ (at $p_b = 20$): this represents a switch from a bamboo to a topologically symmetric two-bubble state, which is one of the states designated as metastable.

As l_2°/l_1° increases, again for intermediate values of l_1°, the topological transformation path $T1^{0}_{cu'}$ becomes more frequent. There is also just one case in figure 8 (specifically for $l_1^\circ = 0.3$ and $l_2^\circ/l_1^\circ = 0.9$) in which following $T1^{0}_{cu'}$ a system manages to undergo an additional transformation afterwards, leading to $T1^{\varnothing*}_{cu'c}$. When that happens (see figure 2 and also section S6(b) in the electronic supplementary material), the system breaks up entirely and stops migrating, while bubbles $\mathcal{B}_1$ and $\mathcal{B}_3$ are detached from each other but connected to the upper channel wall, and bubble $\mathcal{B}_2$ is connected to the lower channel wall.

In the regime of l_1° and l_2°/l_1° in which this occurs, all bubbles are of quite small area [15]. In that case, in the equilibrium state, bubble $\mathcal{B}_2$ in particular needs to be highly elongated in order to span almost the entire channel width but still maintain small area. There is then a significant energetic benefit in detaching $\mathcal{B}_2$ from $\mathcal{B}_1$ and $\mathcal{B}_3$, and allowing each of the bubbles to retreat to their respective channel walls (figure 2). Even though the $T1^{0}_{cu'}$ state is topologically symmetric and hence usually difficult to break, if the bubbles are of such small area that they must also be highly elongated in the $T1^{0}_{cu'}$ state, there is an advantage in reaching the $T1^{\varnothing*}_{cu'c}$ state. Indeed there is a set of minimum bubble areas for the $T1^{0}_{cu'}$ state to be allowed to exist without breaking, with breakage also being sensitive to pressure around that minimum. This is discussed in electronic supplementary material, section S7(a), and the $T1^{\varnothing*}_{cu'c}$ state seen here is actually around that minimum.

As l_1° further increases from intermediate towards large values, particularly for $l_1^\circ = 0.8$ and $l_2^\circ/l_1^\circ = 0.1$, in figure 8 we see a transition from $T1^{b3}_{[\overline{ul'}l]}$ (at $p_b = 10$) to $T1^{0}_{cu'}$ (at $p_b = 20$). For the same $l_2^\circ/l_1^\circ = 0.1$ but now for $l_1^\circ = 0.9$, we see a transition from $T1^{b3}_{[\overline{l'u^!}l]}$ (at $p_b = 10$) to no topological transformation at all (at $p_b = 20$). Although it may seem unusual that subjecting a system to higher

driving pressure prevents rather than induces topological transformation, the behaviour has been seen before by Torres-Ulloa & Grassia [16]. For l_1° and l_2°/l_1° values in this part of the phase diagram, it has been demonstrated that additional steady solution branches are permitted for the original three-bubble topology, but these new branches only appear above a certain pressure [16].

For $l_1^\circ = 0.96$ (the largest l_1° value we consider) and $l_2^\circ/l_1^\circ = 0.2$ we see a transition from $T1_l^{0*}$ (at $p_b = 10$) to $T1_{lu'l}^{b3*}$ (at $p_b = 20$). For the same $l_1^\circ = 0.96$ but values of $l_2^\circ/l_1^\circ > 0.2$, we still, however, observe $T1_l^{0*}$ as the most common topological transformation type. In fact in figure 8 for $p_b = 20$ shows this transformation to be more prevalent than in figure 7 for $p_b = 10$, because cases with $l_2^\circ/l_1^\circ \in [0.8, 0.9]$ have begun undergoing $T1$s as well.

Finally, in figure 8, we still see a reasonably significant region in the phase diagram for which $T1$ transformations are resisted altogether (denoted by $\times$) even up to $p_b = 20$. However, this region has definitely shrunk relative to the $p_b = 10$ case. The principal reason why this region has shrunk is because the path $T1_{cu'}^0$ is now much more frequent.

(iv) Topological transformation paths for $p_b = 40$ and $p_b = 80$

For $p_b = 40$ and $p_b = 80$ (in figures 9 and 10, respectively), for small values of l_1° and a wide range of l_2°/l_1° values, we can again see that the $T1_{[\overline{uc}u]}^{b1}$ is the most common path. On the other hand, for intermediate to large l_1° values and large l_2°/l_1° values, $T1_{cu'}^0$ becomes the most frequent path, particularly at $p_b = 80$. The region (denoted by $\times$) which still manages to resist $T1$ shrinks a great deal.

Transitions between different paths (cases enclosed in boxes) are again observed from figure 8 (for $p_b = 20$) to figure 9 (for $p_b = 40$), and then to figure 10 (for $p_b = 80$). Again these tend to be located within or at least near buffer regions (shown in boldface) in which different $T1$s are competing (see details in section S3(b) in the electronic supplementary material and also [15]). In figure 9, starting with small l_1° values, we note for $l_1^\circ = 0.2$ and $l_2^\circ/l_1^\circ = 0.7$, and also for $l_1^\circ = 0.3$ and $l_2^\circ/l_1^\circ = 0.6$, topological paths change from $T1_{[\overline{uc}u]}^{b1}$ (at $p_b = 20$) to $T1_{[\overline{c}uu]}^{b1}$ or to $T1_{[\overline{c}uu'u]}^{b1*}$ (at $p_b = 40$). For these same l_1° and l_2°/l_1° values, a new transition to yet another path is observed at $p_b = 80$ (figure 10), in which both become $T1_{cu'}^0$.

We now examine both figures 9 and 10, in the domain of small values of l_1° and large values of l_2°/l_1°. As in figure 8 (for $p_b = 20$), cases in which systems reach $T1_{cu'c}^{\varnothing*}$ are again observed. As mentioned earlier, these cases correspond to bubbles with small area retreating to their respective channel walls (see also figure 2), which is energetically favourable for small bubbles. Further discussion of this can be found in the electronic supplementary material, section S7(a).

Moving on to intermediate l_1° values, namely $l_1^\circ \in [0.4, 0.5, 0.6]$ and selected values of $l_2^\circ/l_1^\circ \in [0.1, 0.2, 0.3, 0.4]$, transitions from $T1_{[\overline{uc}u]}^{b1}$ (at $p_b = 20$) to $T1_{[\overline{uc}u'u]}^{b1*}$ and $T1_{[\overline{cu}u'u]}^{b1*}$ (at $p_b = 40$) are observed. For the same values of l_1°, but slightly larger values of l_2°/l_1°, we observe some cases in which $T1_{[\overline{uc}u'u]}^{b1*}$, $T1_{[\overline{c}uu'u]}^{b1*}$ and $T1_{[\overline{c}uu]}^{b1}$ (at $p_b = 20$) become $T1_{cu'}^0$ in figure 9 (at $p_b = 40$).

In figure 10 (for $p_b = 80$), we again observe transitions from $T1_{[\overline{uc}u]}^{b1}$ (at $p_b = 40$) to $T1_{[\overline{uc}u'u]}^{b1*}$ (at $p_b = 80$), specifically for $l_1^\circ \in [0.2, 0.3, 0.4]$ and small to intermediate l_2°/l_1°. For values of l_1° up to 0.6 and a variety of values of l_2°/l_1°, there are also transitions observed from $T1_{[\overline{uc}u'u]}^{b1*}$, $T1_{[\overline{cu}u'u]}^{b1*}$ and $T1_{[\overline{c}uu]}^{b1}$ (at $p_b = 40$), to $T1_{cu'}^0$ (at $p_b = 80$).

On the other hand, in figure 10 for $p_b = 80$, with somewhat larger values of $l_1^\circ \in [0.7, 0.8, 0.9]$ and also values of $l_2^\circ/l_1^\circ \in [0.1, 0.2]$, no topological transformations at all are observed. This includes cases such as $l_1^\circ = 0.7$ and $l_2^\circ/l_1^\circ \in [0.1, 0.2]$ for which $p_b = 40$ in figure 9 (and also $p_b = 20$ with $l_1^\circ = 0.8$ and $l_2^\circ/l_1^\circ = 0.1$ in figure 8) would lead to $T1_{cu'}^0$. Some of these cases that survive intact for large imposed p_b are within the region predicted by Torres-Ulloa & Grassia [15] to have no $T1$ whatsoever (albeit this prediction came from a steady state methodology, not the unsteady methodology used here). Examples are $l_1^\circ \in [0.8, 0.9]$ and $l_2^\circ/l_1^\circ = 0.2$. Other cases, however, such as $l_1^\circ = 0.7$ and $l_2^\circ/l_1^\circ = 0.2$, and also $l_1^\circ \in [0.7, 0.8, 0.9]$ and $l_2^\circ/l_1^\circ = 0.1$, are outside that region, so the methodology of Torres-Ulloa & Grassia [15] would predict $T1$. As already mentioned though, it is known via [16] that in cases such as these, a new steady state solution branch avoiding

topological transformation is still possible, but this branch only appears beyond a certain driving pressure: as such the methodology used in [15] would not detect it.

Considering now $l_1^\circ = 0.96$ (i.e. the largest l_1° value studied here), although no differences are seen between figures 8 and 9 (comparing $p_b = 20$ and $p_b = 40$, respectively), as we move from $p_b = 40$ (in figure 9) to $p_b = 80$ (in figure 10), we see a significant number of changes. In particular, numerous $T1_l^{0*}$ transformations are replaced by $T1_{cu'}^{0}$ for $l_2^\circ/l_1^\circ \in [0.3, 0.4, 0.5, 0.6, 0.7, 0.9]$, albeit not for $l_2^\circ/l_1^\circ = 0.8$. In effect one type of metastable state (shown in figure 5) is being replaced by another (in figure 2). Finally, again for $l_1^\circ = 0.96$ and but now for small values of $l_2^\circ/l_1^\circ \in [0.1, 0.2]$, we see a transition from $T1_{lu^{\dagger}l}^{b3*}$ (at $p_b = 40$) to $T1_{l'}^{0'}$ (at $p_b = 80$). A bamboo endpoint state (figure 5) is thereby being replaced by a metastable one (figure 4).

(v) Number of cases for each topological transformation path

Note that for $p_b \in [10, 20, 40, 80]$ at least, all the states that undergo topological transformation whatsoever eventually end up with zero asymmetry index, i.e. equal numbers of propagating films attached to the upper and lower channel walls. Even those cases with no films migrating at all (denoted $T1_{cu'c}^{\varnothing*}$) have an asymmetry index of zero by default since there are no propagating films to count on either wall.

Out of the propagating states, a large number of them are bamboo states, designated with superscript $b1$ (or $b1*$), or else $b3$ (or $b3*$). These are topological 'endpoint states' that can propagate at any velocity without deforming and hence without undergoing any further $T1$. However, the number of such cases decreases as p_b increases, giving way for the most part to $T1_{cu'}^{0}$ instead, which becomes very common indeed. The exact numbers for each of the different states is shown in table 1. Note that some states (e.g. the $T1_{cc}^{\varnothing}$ state or the $T1_{lu^{\dagger}u}^{b2}$ state) are not seen in table 1 as they do not occur for the limited set of pressures considered there.

Transitions between the different states with varying pressure are discussed next, and are also discussed further in §4b.

(vi) Number of transitions between topological transformation paths

In table 2, we compare states that change their $T1$ transformation path between $p_b = 10$ and $p_b = 20$, between $p_b = 20$ and $p_b = 40$, and between $p_b = 40$ and $p_b = 80$. Specifically we quantify at the higher pressure, cases in which the transformation type seen at the lower pressure was different. We also include cases in which there is no transformation (denoted by $\times$) at the higher pressure but there is a transformation at the lower pressure. Cases in which there are topological transformations at higher pressure but not at low pressure are specifically excluded, as it is common that a threshold driving pressure is needed before a $T1$ is induced. We also count not just the number of transitions between transformation paths, but also the number of them taking place within buffer regions in which, as predicted by Torres-Ulloa & Grassia [15], various $T1$ types are known to compete (see section S3 in the electronic supplementary material and in particular section S3(b)). The buffer region cases are shown within table 2 to the right of '|'.

It is evident from the table that the majority of the transitions between transformation paths are observed at large pressures (from $p_b = 40$ to $p_b = 80$), and moreover switching into $T1_{cu'}^{0}$ is common. At lower pressures, fewer transitions between different topological transformation paths are seen, however, out of those that do occur, a significant number of them are in the aforementioned buffer regions. Therefore, if a transition between transformation paths takes place at all, it is likely that it happens in the buffer regions. Conversely, if a given system falls within these buffer regions, it is also likely that a transition between topological paths will occur.

To conclude, looking at figures 7–10 and also table 1, we can see that topological transformations only rarely happen singly, but more often happen as a sequence in a path resulting eventually in a state that is topologically symmetric. More insights into why particular sequences of topological transformations occur can be obtained by examining the energy of the

Table 2. Via unsteady state simulation for different pressures, out of a sample for each pressure of 90 cases with various l_1° and l_2°/l_1° values, it is shown how many transitions between topological transformation paths are seen between two pressures. The table is sorted according to the state into which the system switches. Far fewer than the total 90 cases considered exhibit transitions between topological paths between the pressures shown. The values to the right of the '|', indicate which of the transitions between different topological paths are (according to Torres-Ulloa & Grassia [15]) in buffer regions in which different $T1$ types compete. Note that out of 90 cases in total, just nine of them fall into buffer regions (as can be seen in figure 10 by counting up the boldface cases). Not all nine of these buffer region cases, however, exhibit transitions between topological paths between the pressures shown.

p_b	10–20	20–40	40–80
$T1^{b1}_{[\overline{uc}u]} \rightarrow T1^{b1}_{[\overline{cu}u]}$	1|1	1|1	0|0
$T1^{b1}_{[\overline{uc}u]} \rightarrow T1^{b1*}_{[\overline{cu}u'u]}$	1|1	2|1	0|0
$T1^{b1}_{[\overline{uc}u]} \rightarrow T1^{b1*}_{[\overline{uc}u'u]}$	2|1	5|0	6|0
$T1^{b1}_{[\overline{uc}u]} \rightarrow T1^{0}_{cu'}$	2|0	0|0	1|1
$T1^{b3}_{[\overline{ul'l}]} \rightarrow T1^{0}_{cu'}$	1|1	0|0	0|0
$T1^{b1}_{[\overline{cu}u]} \rightarrow T1^{0}_{cu'}$	0|0	1|1	1|1
$T1^{b1*}_{[\overline{cu}u'u]} \rightarrow T1^{0}_{cu'}$	0|0	1|1	2|1
$T1^{b1*}_{[\overline{uc}u'u]} \rightarrow T1^{0}_{cu'}$	0|0	2|1	3|0
$T1^{0*}_{l} \rightarrow T1^{0}_{cu'}$	0|0	0|0	6|1
$T1^{0*}_{l} \rightarrow T1^{b3*}_{lu^{\dagger}l}$	1|0	0|0	0|0
$T1^{b3*}_{lu^{\dagger}l} \rightarrow T1^{0'}_{l'}$	0|0	0|0	2|0
$T1^{b3}_{[\overline{l'u^{\dagger}l}]} \rightarrow \times$	1|0	0|0	0|0
$T1^{0}_{cu'} \rightarrow \times$	0|0	1|1	2|1
total transitions	9|4	13|6	23|5

three-bubble system, which in this context is just the sum of all film lengths. This is discussed in section S9 in the electronic supplementary material, where it turns out that attaining topological symmetry also enables energy to relax. Full details are given in the electronic supplementary material, section S9.

(b) Statistics of $T1$ behaviour for varying imposed pressures

After having examined the $T1$ behaviour in detail for specific p_b values over the complete l_1° and l_2°/l_1° domain (see figures 7–10, and also tables 1 and 2), in figure 11 we show the system behaviour in a more general statistical fashion albeit for many more pressures than before. Specifically what we show is, for any given integer value of the imposed back pressure varying from $p_b = 0$ to $p_b = 80$, the number of occasions on which each topological transformation path (figures 2–5) is realized for systems within the parameter space $l_1^\circ \in [0.1, 0.2, \ldots, 0.9, 0.96]$ and $l_2^\circ/l_1^\circ \in [0.1, 0.2, \ldots, 0.9]$ (90 cases in total for each p_b, see data in section S8 in the electronic supplementary material). Results are discussed below.

We note from figure 11*a* that the majority of the systems show no $T1$ at all for small p_b values (see solid line). However, for systems that do exhibit $T1$ for small p_b, the preferred path corresponds to $T1^{b1}_{[\overline{uc}u]}$ (see dashed line in figure 11*a*). As p_b increases, however, roughly for values of $p_b > 20$, the preferred path becomes $T1^{0}_{cu'}$ (see dash-dotted line in figure 11*a*), while the number of $T1^{b1}_{[\overline{uc}u]}$ cases decreases. Roughly for $p_b > 20$ also, $T1^{0}_{cu'}$ becomes more common than having no

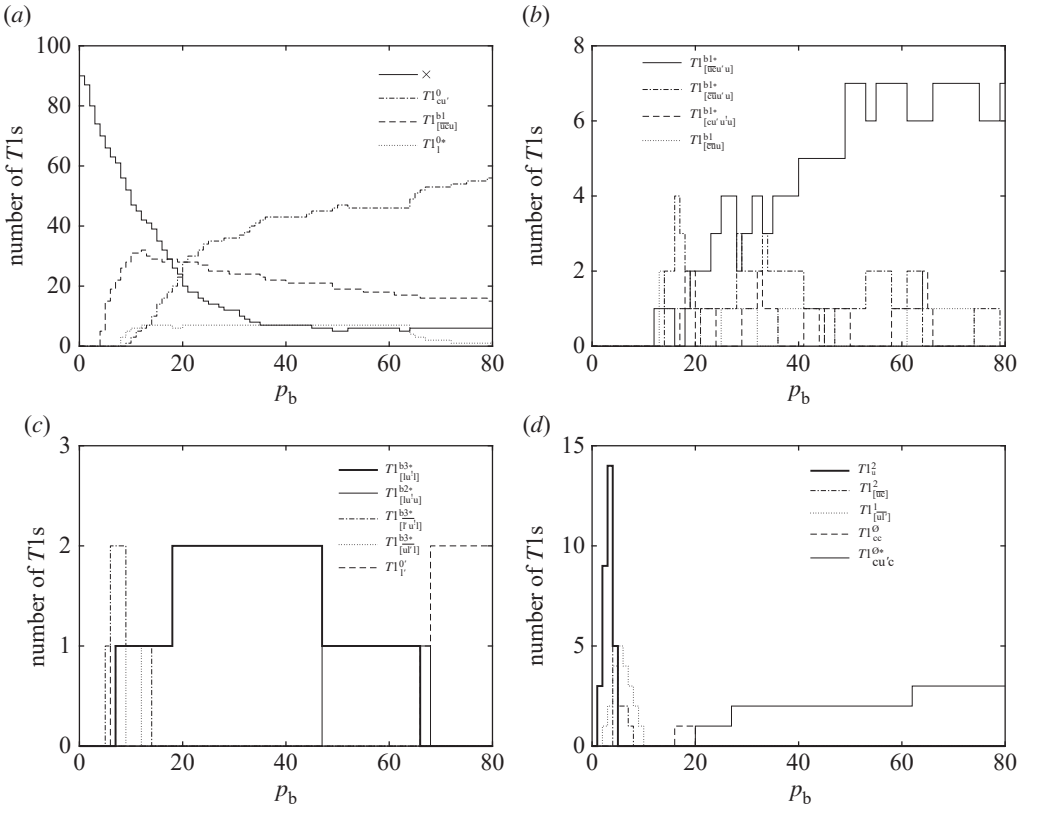

Figure 11. Number of instances of topological transformation paths for each imposed back pressure $p_b \in [0, 1, \ldots, 80]$. For each p_b value we show the number of cases within the parameter space $l_1^\circ \in [0.1, 0.2, \ldots, 0.9, 0.96]$ and $l_2^\circ/l_1^\circ \in [0.1, 0.2, \ldots, 0.9]$ (i.e. 90 cases in total for each pressure). In (*a*) we show the most frequent cases (including $\times$ which means no *T*1), in (*b*) we show the various *b*1 and *b*1∗ bamboo states, in (*c*) we show the *b*3, *b*3∗, *b*2 and $T1^{0'}_{l'}$ states, and finally in (*d*) we show first cases that end in a topologically asymmetric state, namely $T1^{2}_{u}$, $T1^{2}_{[\overline{uc}]}$, $T1^{1}_{[\overline{ul'}]}$, and also cases in which the structure breaks and stops propagating ($T1^{\emptyset}_{cc}$ and $T1^{\emptyset*}_{cu'c}$ paths).

*T*1 at all. Topological path $T1^{0*}_{l}$ also increases in frequency for small p_b but then stays at constant frequency for a wide range of p_b values (see dotted line in figure 11*a*), and finally its frequency starts decreasing for large p_b values.

In figure 11*b* on the other hand, we again show the number of topological transformation paths (out of 90 in total) for each different p_b, but considering those paths leading to various single-bubble bamboo *b*1 and *b*1∗ states not already plotted in figure 11*a*. Here we can see topological paths, such as $T1^{b1*}_{[\overline{cu}u'u]}$ (dash-dotted line), $T1^{b1*}_{[cu'u^1u]}$ (dashed line) and $T1^{b1}_{[\overline{cu}u]}$ (dotted line), which are observed intermittently over the studied p_b domain: again, however, there are seldom more than just a couple of these paths at any given p_b. On the other hand, we also observe from figure 11*b* that the number of $T1^{b1*}_{[\overline{uc}u'u]}$ (solid line) cases increases as p_b increases.

In figure 11*c*, we show some of the very infrequent paths, noting that out of 90 cases total considered at each pressure, each of the cases here occurs at most a couple of times. Many of the paths here lead to bamboo states. The topological path $T1^{b3*}_{lu^1l}$ is not seen for very small or very large p_b values, but is found to persist over a wide domain of intermediate p_b values (see the thick solid line in figure 11*c*). Topological paths $T1^{b3}_{[l'u^1l]}$ and $T1^{b3}_{[\overline{ul'}l]}$ are also seen but just for small p_b values (see the dash-dotted line and dotted line, respectively, in figure 11*c*). Topological path $T1^{b2}_{lu^1u}$ (solid line) is observed over just part of the studied p_b domain, excluding, however, small and very large p_b values. Finally, topological path $T1^{0'}_{l'}$ (giving a metastable state, rather

than a bamboo) is observed for large p_b values (and for at least one small p_b value as well), but not for intermediate values (see the dashed line in figure 11*c*).

Figure 11*d* considers cases that either end up topologically asymmetric, or else break apart completely and do not propagate at all. Topological states $T1^2_u$ are seen in figure 11*d* (see the thick solid line), however, just for small domains of p_b at relatively low pressures. It is clear then that the $T1^2_u$ state can sometimes be more resistant to topological transformations than the original three-bubble staircase structure was. However, the $T1^2_u$ is clearly not resilient to topological transformations in absolute terms, since none of the $T1^2_u$ states survive out to more than a few units of p_b. Other topologically asymmetric paths, such as $T1^2_{[\overline{uc}]}$ and $T1^1_{[\overline{ul'}]}$, are only ever observed for small values of p_b (see the dash-dotted and dotted line, respectively, in figure 11*d*). Regarding cases that break up and do not propagate at all, in figure 11*d* we sometimes see $T1^{\emptyset}_{cc}$ for small p_b (dashed line), but never more than one at any given p_b, and none at all as p_b increases. Meanwhile, topological path $T1^{\emptyset *}_{cu'c}$ (solid line in figure 11*d*) is not seen for $p_b < 20$, but becomes a little more frequent as p_b increases.

Looking at figure 11 overall, remembering we start from a staircase with a topological asymmetry index of unity, there is a clear preference for eventually reaching topologically symmetric states (assuming any topological transformations happen at all). Nonetheless, during the course of the evolution, the level of topological asymmetry (i.e. the value of the asymmetry index) can still sometimes increase, temporarily at least. For instance, this happens with paths beginning with $T1^2_{[\overline{uc}]}$ as the first two steps, which are seen often (as well as for paths beginning with $T1^2_{[\overline{cu}]}$, which are seen occasionally also). Paths beginning in this fashion tend to be favoured for small l_1° and small l_2°/l_1° (figures 7–10). Bubbles $\mathcal{B}_1$ and $\mathcal{B}_3$ are then of small area, but bubble $\mathcal{B}_2$ is larger. On the other hand, a different path $T1^0_{cu'}$ tends to be favoured for larger l_1° and larger l_2°/l_1° (again see figures 7–10), with bubbles $\mathcal{B}_1$ and $\mathcal{B}_3$ then being larger in area, while bubble $\mathcal{B}_2$ can be smaller. There is certainly no temporary increase in asymmetry index in this particular case. Moreover as driving pressure p_b increases (and thus velocity and hence viscous drag likewise increase to compensate), systems can switch away from paths beginning with $T1^2_{[\overline{uc}]}$ (or $T1^2_{[\overline{cu}]}$) as the first two steps, towards $T1^0_{cu'}$ instead. Hence temporary increases in topological asymmetry become less common in the high driving pressure scenario.

(c) Mobility of final topological states

For each different set of bubble sizes that we have considered, and for each different pressure applied, we either do not have any $T1$, or else systems undergo what is typically a sequence of $T1$s to reach a final topological state. Here we compute the mobility (i.e. ratio of final propagation velocity to driving pressure, namely v/p_b) for various final states. Short-lived intermediate states are, therefore, omitted from this analysis. Whenever the final topology changes, the mobility also changes, i.e. mobility will be sensitive to the particular sequence of topological transformations (if any) that occurs.

(i) Determining mobility for high driving pressures and/or high velocity

Both velocity and pressure are taken to be dimensionless quantities here (see the electronic supplementary material, section S1, for details of how the system is made dimensionless, and in particular the electronic supplementary material, equation (S1.2), which is the dimensionless governing equation, also given earlier as equation (2.1)). Hence mobility is likewise taken to be dimensionless. For simplicity, we compute mobilities just for systems moving in the high driving pressure limit, or equivalently in the limit of high propagation velocity [25]. In this particular limit and in the dimensionless system studied here, the pressure difference Δp across any given film turns out to equal $v\cos\phi$, where v is apparent propagation velocity along the channel (uniform over the entire structure in the final state) and ϕ is the angle that the film tangent makes to the vertical between lower and upper channel walls: see [25] for details. Note that in the high driving pressure limit, ϕ can vary from film to film, but is asymptotically spatially uniform along

any individual film except in a small region at each film's upstream end [15,19]. If we consider pressure differences film by film, and sum them for each film that is crossed moving across the entire structure from upstream to downstream, we obtain the imposed pressure p_b. Based on this, the mobility v/p_b is then the reciprocal of the sum of the $\cos\phi$ values. The mobility is lower when more films are crossed. Also films that are oriented with their tangent pointing directly across the channel from wall to wall have more impact on reducing mobility than films that are oriented obliquely.

All of this allows us in what follows to obtain analytical estimates of mobility, and moreover the resulting mobilities in this particular high driving pressure limit [25] turn out to depend solely on topology, not on individual bubble sizes. We can also calculate a mobility in this fashion even for the original three-bubble topology, supposing it reaches a geometrically invariant state that resists $T1$ even at high driving pressure [15]. We can also evaluate mobilities for metastable systems (with topological asymmetry index of zero, see section S6(e) in the electronic supplementary material for details) reaching various final states $T1^0_{cu'}$, $T1^{0'}_{l'}$ and $T1^{0*}_{l}$ (see figures 2, 4 and 5, respectively). Bamboo structures (see section S6(c) in the electronic supplementary material), namely $b1$ (or $b1*$), $b2$, $b3$ (or $b3*$), are also considered here (figures 2–6). These bamboo states (which can be reached by various topological paths) once realized move at any driving pressure without changing either their topology or geometry. Their mobility is, therefore, independent of whether it is computed in the high driving pressure limit or at any other p_b.

(ii) Mobility of various structures for high driving pressure and/or high velocity

Mobility of bamboo states is easy to determine because no films are oblique. We can, therefore, readily demonstrate that the (dimensionless) mobility of the $b3$ (or $b3*$) bamboo structures is 1/4 (four films to cross from upstream to downstream), whereas by analogous arguments the mobility of the $b2$ bamboo is 1/3, and the mobility of the $b1$ (or $b1*$) bamboo is 1/2. Based on Torres-Ulloa & Grassia [15], the mobility of the original three-bubble staircase structure, assuming it reaches a high driving pressure without breaking up, is also 1/2 (at least two films to cross upstream to downstream).

On the other hand, the mobility of the $T1^0_{cu'}$ state (again in the high driving pressure or high velocity limit) can be determined by considering that this corresponds to crossing two films, but one of them (at the upstream end) being oblique with an orientation angle of $\pi/6$ between the film tangent and the vertical (see figure S5*b* in the electronic supplementary material for a sketch). Therefore, based on the aforementioned rule of the reciprocal of the sum of the cosines, we find that the dimensionless mobility of the $T1^0_{cu'}$ state corresponds to $(1+\sqrt{3}/2)^{-1} \approx 0.5359$. States $T1^{0*}_{l}$ and $T1^{0'}_{l'}$ topologically consist of films that are propagating within state $T1^0_{cu'}$ plus a film spanning across the channel downstream in the case of $T1^{0*}_{l}$, or upstream in the case of $T1^{0'}_{l'}$. Therefore, in each case there are three films to cross, but one of them being oblique to the channel. Hence the mobility of both states $T1^{0*}_{l}$ and $T1^{0'}_{l'}$ is $(2+\sqrt{3}/2)^{-1} \approx 0.3489$. What is interesting from the above analysis is that the $T1^0_{cu'}$ state is the one most commonly selected (particularly at higher driving pressures) and is also the state with the highest mobility.

5. Conclusion

We have studied the evolution over time of a two-dimensional three-bubble evolution as it flows within a confined straight channel, due to an imposed back pressure p_b. Evolution from the equilibrium topology is realized via unsteady state simulation with the viscous froth model. The equilibrium system itself is defined by fixing the distances from vertices to the upper channel wall, either l_1° (for vertex V_1 and V_3) or l_2° (for vertex V_2, with $l_2^\circ < l_1^\circ$). Distances l_1° and l_2°/l_1° are, therefore, used as surrogates of bubble areas. As in a previous study [16], here we consider a wide domain for l_1° and l_2°/l_1°, namely $l_1^\circ \in [0.1, 0.2, \ldots, 0.9, 0.96]$ and $l_2^\circ/l_1^\circ \in [0.1, 0.2, \ldots, 0.9]$ (90 cases in total). Each case is considered by suddenly imposing a dimensionless back pressure somewhere in the domain $p_b \in [0, 1, \ldots, 80]$, with p_b considered in integer increments.

At sufficient imposed back pressure, topological transformations occur such that bubbles in the structure rearrange. How the system evolves up to the first topological transformation has been studied before [16], including via the unsteady state simulation technique as employed here. Up to four different $T1$s were found for different combinations of l_1° and l_2°/l_1°, and also for different imposed p_b values. Our unsteady state simulation methodology nevertheless also allows us to look beyond the first transformation, towards sequences of transformations, and thereby to elucidate topological transformation paths: this is what has been achieved here. Typically the transformation paths involve systems evolving through a sequence of short-lived intermediate states before settling into an eventual final topological configuration. Once the final topological configuration is identified, it is also possible to identify the mobility (ratio of velocity to pressure imposed) for each of the final configurations. Certain configurations have been found to be more mobile than others.

We defined a topological asymmetry index based on the difference between numbers of films connected to the upper and lower channel wall, counting only moving films, omitting bubbles that have been left behind and are no longer moving. In the initial staircase topology, the asymmetry index was necessarily non-zero based on having three (i.e. an odd number of) bubbles present. Topological asymmetry can drive topological transformation on the basis that having more films on one side of a structure than the other leads to more viscous drag on that side and hence bubbles falling behind the rest of the structure.

That the asymmetry index is a useful measure was demonstrated by the fact that for almost all the topological transformation paths that we examined, the asymmetry index at the end of the transformation path turned out to be zero. There were, however, distinct ways in which the asymmetry index could become zero.

One possibility was for the system to reach what we called a topological endpoint state, in which the structure has arranged itself into a very simple configuration such that any films that propagate will do so at any velocity whatsoever without needing to deform (and therefore without any possibility of further $T1$). Typically the endpoint states involve bamboo type structures, possibly with one or more bubbles left behind on channel walls.

Another option was for the system to reach what we called a topologically symmetric metastable state (albeit not an endpoint state). In such states, even though further deformation (depending on imposed driving pressure) and further transformations remain possible in principle, they tend not to happen in practice, since the symmetry allows the system to propagate over a wide domain of driving pressures without breaking. Typically in such states, two bubbles are stacked across the channel, with a third one either immediately ahead of them or immediately behind them or else left behind altogether.

Indeed a very commonly occurring example of a topologically symmetric state was the $T1^0_{cu'}$ state (figure 2), which happened over a wide domain of bubble sizes (figures 7–10), and was especially common at large imposed driving pressures. This state was also found to offer the highest mobility compared with the other alternatives. To reach this state, bubbles must first reconnect via a vertex–vertex collision $T1^1_c$ and then a bubble is shed from the back of the structure via a $T1_{u'}$ to achieve topological symmetry.

It is interesting to speculate what might happen to a long train of bubbles rather than just the three-bubble state considered here. The experimental study of Drenckhan *et al.* [14] showed a sequence of $T1_c$ transformations (i.e. a sequence of vertex–vertex collisions) working its way along the train. Admittedly the cited study involved geometric asymmetry (flow around a bend) rather than topological asymmetry as is considered in the present work. However, a chain of $T1_c$ transformations plus a $T1_{u'}$ could ensure topological symmetry. Specifically the chain of $T1_c$ transformations (vertex–vertex collisions) would allow bubbles on the side of the channel with fewer films and thereby less drag to overtake bubbles on the other side with more films and thereby more drag. Meanwhile the $T1_{u'}$ (shedding a bubble from the back of a train containing an odd number of bubbles, leaving that backmost bubble behind) would ensure that only an even number of bubbles continue to propagate, hence permitting topological symmetry. This then would seem to be a suitable way to generalize the $T1^0_{cu'}$

state that is commonly observed in the present work to a situation with more than three bubbles.

Finally it is interesting to draw a speculative analogy between the systems studied in this work (clusters of bubbles moving in a microfluidic channel) and the field of sub-atomic, high energy physics [26]. We have identified a bubble structure which if subjected to enough 'energy' (i.e. enough imposed pressure) breaks up through a sequence of short-lived intermediate states, eventually finding itself in a more favourable topological configuration. However, the sequence of intermediate states and the eventual configuration that is reached depends on the 'energy' (i.e. the imposed pressure) to which systems are subjected in the first place, just as would also happen in high energy physics. In the context of foam physics, the simple lens of Green *et al.* [19] is the 'hydrogen atom' (i.e. the simplest structure containing the various elements of a foam), whereas the three-bubble case becomes the 'three-bubble problem' [15,16] (i.e. the situation at which complexity first onsets). By analogy then, unsteady state dynamics with multiple topological transformations for three-bubble systems (or indeed for more general N-bubble systems) could perhaps be considered the 'large hadron collider' of foam physics.

Data accessibility. All results presented here are reproducible by procedures or numerical algorithms (accessible via https://doi.org/10.15129/ba161821-450d-44dd-93b4-db8787cb9c18), which are also detailed in the article and in the electronic supplementary material [27].

Authors' contributions. C.T.-U.: formal analysis, methodology, software, visualization, writing—original draft, writing—review and editing; P.G.: conceptualization, formal analysis, funding acquisition, supervision, writing—review and editing.

Both authors gave final approval for publication and agreed to be held accountable for the work performed therein.

Conflict of interest declaration. We declare we have no competing interests.

Funding. C.T.-U. and P.G. acknowledge support from EPSRC grant EP/V002937/1. C.T.-U. acknowledges support from Centro de Investigación, Innovación y Creación UCT (CIIC-UCT).

Acknowledgements. C.T.-U. acknowledges S. Cox, D. Vitasari, E. Mas-Hernández, G. Montecinos and J. Hernández-Montelongo for hosting research visits during which useful discussions took place.

References

1. Zhan F, Youssef M, Shah BR, Li J, Li B. 2022 Overview of foam system: natural material-based foam, stabilization, characterization, and applications. *Food Hydrocoll.* **125**, 107435 (doi:10.1016/j.foodhyd.2021.107435)
2. Stevenson P. 2012 *Foam engineering: fundamentals and applications*. Chichester, UK: John Wiley & Sons.
3. Jia X, Mowatt G, Burr JM, Cassar K, Cook J, Fraser C. 2007 Systematic review of foam sclerotherapy for varicose veins. *Br. J. Surg.* **94**, 925–936. (doi:10.1002/bjs.5891)
4. Kotb MM, Shakiban HK, Sawaby AF. 2013 Foam treatment for varicose veins; efficacy and safety. *Alex. J. Med.* **49**, 249–253. (doi:10.1016/j.ajme.2012.11.003)
5. Hirasaki GJ, Lawson JB. 1985 Mechanisms of foam flow in porous media: apparent viscosity in smooth capillaries. *Soc. Petrol. Eng. J.* **25**, 176–190. (doi:10.2118/12129-PA)
6. Roberts TG, Cox SJ, Lewis AL, Jones SA. 2021 Characterisation and optimisation of foams for varicose vein sclerotherapy. *Biorheology* **57**, 77–85. (doi:10.3233/BIR-201004)
7. Kovscek AR, Bertin HJ. 2003 Foam mobility in heterogeneous porous media. *Transp. Porous Media* **52**, 17–35. (doi:10.1023/A:1022368228594)
8. Cantat I, Kern N, Delannay R. 2004 Dissipation in foam flowing through narrow channels. *Europhys. Lett.* **65**, 726–732. (doi:10.1209/epl/i2003-10169-0)
9. Jones SA, Dollet B, Méheust Y, Cox SJ, Cantat I. 2013 Structure-dependent mobility of a dry aqueous foam flowing along two parallel channels. *Phys. Fluids* **25**, 063101 (doi:10.1063/1.4811178)
10. Géraud B, Jones SA, Cantat I, Dollet B, Méheust Y. 2016 The flow of a foam in a two-dimensional porous medium. *Water Resour. Res.* **52**, 773–790. (doi:10.1002/2015WR017936)
11. Cantat I, Delannay R. 2003 Dynamical transition induced by large bubbles in two-dimensional foam flows. *Phys. Rev. E* **67**, 031501 (doi:10.1103/PhysRevE.67.031501)

12. Cantat I, Delannay R. 2005 Dissipative flows of 2D foams. *Eur. Phys. J. E* **18**, 55–67. (doi:10.1140/epje/i2004-10154-5)
13. Cantat I, Poloni C, Delannay R. 2006 Experimental evidence of flow destabilization in a two-dimensional bidisperse foam. *Phys. Rev. E* **73**, 011505 (doi:10.1103/PhysRevE.73.011505)
14. Drenckhan W, Cox SJ, Delaney G, Holste H, Weaire D, Kern N. 2005 Rheology of ordered foams: on the way to discrete microfluidics. *Colloids Surf. A* **263**, 52–64. (doi:10.1016/j.colsurfa.2005.01.005)
15. Torres-Ulloa C, Grassia P. 2022 Viscous froth model applied to the motion of two-dimensional bubbles in a channel: three-bubble case. *Proc. R. Soc. A* **478**, 20210801 (doi:10.1098/rspa.2021.0642)
16. Torres-Ulloa C, Grassia P. 2022 Viscous froth model applied to the dynamic simulation of two-dimensional bubbles in a channel: three-bubble case. *Proc. R. Soc. A* **478**, 20220487 (doi:10.1098/rspa.2022.0487)
17. Grassia P, Montes-Atenas G, Lue L, Green TE. 2008 A foam film propagating in a confined geometry: analysis via the viscous froth model. *Eur. Phys. J. E* **25**, 39–49. (doi:10.1140/epje/i2007-10262-8)
18. Osei-Bonsu K, Shokri N, Grassia P. 2016 Fundamental investigation of foam flow in a liquid-filled Hele-Shaw cell. *J. Colloid Interface Sci.* **462**, 288–296. (doi:10.1016/j.jcis.2015.10.017)
19. Green TE, Bramley A, Lue L, Grassia P. 2006 Viscous froth lens. *Phys. Rev. E* **74**, 051403 (doi:10.1103/PhysRevE.74.051403)
20. Weaire D, Phelan R. 1996 The physics of foam. *J. Phys.: Condens. Matter* **8**, 9519–9524. (doi:10.1088/0953-8984/8/47/055)
21. Kern N, Weaire D, Martin A, Hutzler S, Cox SJ. 2004 Two-dimensional viscous froth model for foam dynamics. *Phys. Rev. E* **70**, 041411 (doi:10.1103/PhysRevE.70.041411)
22. Embley B, Grassia P. 2011 Viscous froth simulations with surfactant mass transfer and Marangoni effects: deviations from Plateau's rules. *Colloids Surf. A* **382**, 8–17. (doi:10.1016/j.colsurfa.2011.01.013)
23. Vitasari D, Cox S, Grassia P, Rosario R. 2020 Effect of surfactant redistribution on the flow and stability of foam films. *Proc. R. Soc. A* **476**, 20190637 (doi:10.1098/rspa.2019.0637)
24. Grassia P, Embley B, Oguey C. 2012 A Princen hexagonal foam out of physicochemical equilibrium. *J. Rheol.* **56**, 501–526. (doi:10.1122/1.3687442)
25. Cox SJ, Weaire D, Mishuris G. 2009 The viscous froth model: steady states and the high-velocity limit. *Proc. R. Soc. A* **465**, 2391–2405. (doi:10.1098/rspa.2009.0057)
26. Perkins DH, Perkins DH. 2000 *Introduction to high energy physics*. Cambridge, UK: Cambridge University Press.
27. Torres-Ulloa C, Grassia P. 2023 Viscous froth model applied to multiple topological transformations of bubbles flowing in a channel: three-bubble case. Figshare. (doi:10.6084/m9.figshare.c.6708076)